NTNU
Norwegian University of
Science and Technology

Geomagnetic Induced Current Effects on Power Transformers

Benjamin Røen

Master of Energy and Environmental Engineering
Submission date: June 2016
Supervisor: Hans Kristian Høidalen, ELKRAFT
Co-supervisor: Lars Lundgaard, SINTEF
Trond Magne Ohnstad, Statnett

Norwegian University of Science and Technology
Department of Electric Power Engineering

Problem Description

Solar storms are inevitable and have a number of negative effects on technological systems, the power grid being no exception. High geoelectric field values due to severe geomagnetic storms cause geomagnetic induced currents to flow in conducting structures of the power system. The geomagnetic induced currents will enter and leave the power grid through the neutral grounding of power transformers. This may cause half-cycle saturation of the transformer core, which in turn leads to high levels of harmonics in transformer currents, increased transformer reactive power consumption and heating of transformer. Furthermore, flow of geomagnetic induced current in power transformers can cause tripping of components with to sensitive safety limits and damaging of transformer. Cascading failure may be initiated, which in turn can lead to blackouts and loss of production.

The effects of geomagnetic induced current on power transformers should be further investigated. In addition, a basic knowledge of solar storms, geomagnetic induced currents and their effects on power transformers and power systems should be provided.

Preface

The Master's thesis is about geomagnetic induced current effects on power transformers during geomagnetic storms, and is written at NTNU as part of the study program Energy and Environmental Engineering. The work was carried out during the spring semester of 2016. The idea to the project was brought up in the context of a cooperation project involving Statnett, Sintef Energy and NTNU, among others. The mission of the cooperation project is to understand how the geomagnetic storms affect the Norwegian power grid, and how to develop best practice mitigation measures to reduce or prevent damage from geomagnetic induced currents.

The work is aimed to help people with an electrical engineer background to better understand the power transformers response to geomagnetic induced current, in addition to providing a greater understanding of solar storms and effects of space weather on the Norwegian power grid.

Trondheim, 2016-06-10

Benjamin Røen

Acknowledgment

I would like to thank the following persons for all their help, motivation and support during this study:

First, I would like to thank my parents, my big brother and my big sister for always believing in me and supporting me no matter what I have tried to accomplish. With your love and encouragement, I have been able to follow my dreams. And without your guidance I could never have reached this far.

My beloved boyfriend, Sigurd. You are my love and inspiration. You are my rock. Without your advice and patience during this work I would never have made it.

Finally, I would like to thank my supervisor, Prof. Hans Kristian Høidalen, for your enlightening suggestions and encouragement. I greatly appreciate your guidance and helpful advice in using ATPDraw, and I consider myself very fortunate for being able to work with such a talented supervisor.

B.R.

Abstract

This project paper is a study on the solar storms and their effects on power systems. The main focus will be on geomagnetic induced currents and their effects on power transformers, i.e. half-cycle saturation, increased reactive power consumption, high levels of harmonics and heating. The project report may be divided into two parts. The first part presents the litterature rewiev on solar storms and geomagnetic induced currents, and their effects on power transformers and power systems. The second part concerns the simulation setup in ATPDraw and the corresponding results. First, the circuit diagrams and power transformer models are explained. Then, measurement methods are described and results are given and discussed.

Solar storms are inevitable and has a number of negative effects on technologial systems. High geoelectric field values due to severe geomagnetic storms cause geomagnetic induced currents to flow in conducting structures of the power system. For power lines, the geomagnetic induced current enters and leaves through the neutral grounding of transformers.

The solar activity varies with a frequency of approximately 11 years. This periodicity is known as the sunspot cycle because it is closely related to the number of dark spots on the surface of the sun.

Geomagnetic induced current flow can cause tripping of components with to sensitive safety limits and damaging of transformer. Cascading failure may be initiated, which in turn can lead to blackouts and loss of production.

Development of mitigation strategies and risk assessment should be carried out. Key factors are space weather prediction, modifications of the power system and emergency operation plans.

Factors influencing geomagnetic induced current values have also been reviewed providing a tool to discuss the probability of and area to be exposed to adverse effects due to severe geomagnetic storms or not.

It turned out to be a challenge to represent the geomagnetic induced current by using a voltage source. Thus, results are only given for the circuit diagram where the geomagnetic induced current is represented by a DC current source connected to the HV

winding of the power transformer of interest. The results indicates that the three-phase three-legged transformer are less susceptible to geomagnetic induced current effects than the three-phase five-legged transformer. Furthermore, having a delta connected tertiary winding gives higher steady-state values in terms of reactive power consumption and current flowing into the high voltage side of the transformer. On the other hand, an interesting observation is that the reactive power consumption and transformer current have a smaller time step. Consequently, not having a delta connected tertiary winding results in higher reactive power consumption and transformer current to begin with. On the basis of the results the three-phase three-legged transformer with a delta connected tertiary winding seems to be the best choice during large geomagnetic disturbances.

Sammendrag

Masteroppgaven er et studie av solstormer og deres effekter på kraftnettet. Hovedfokuset vil være på geomagnetisk induserte strømmer og deres effekter på transformatorer. Effektene skyldes at transformatoren går i metning, som igjen fører til økt reaktivt konsum, høye verdier av harmoniske strømmer og overoppheting av transformatoren. Prosjektrapporten kan deles inn i to. Prosjektrapporten kan deles inn i to. Den første delen presenterer litteratursøket knyttet til solstormer og geomagnetisk induserte strømmer, og deres effekt på transformatorer og kraftsystemer. Den andre delen omhandler simuleringoppsettet i ATPDraw og tilsvarende resultater. Først blir koblingsskjemaer og transformator modeller forklart. Deretter blir målemetoder beskrevet, og resultatene er angitt og diskutert.

Solstormer er ikke til å unngå, og har en rekke negative effekter på teknologiske systemer. Høye geoelektriske felt på grunn av kraftige geomagnetiske stormer fører til at geomagnetisk induserte strømmen flyter gjennom kraftnettet. Den geomagnetisk induserte strømmen kommer opp i og forlater kraftledninger gjennom nøytraljordinger av transformatorer.

Solens aktivitet varierer med en syklus på omtrent 11 år. Denne syklusen er kjent som solflekksyklus fordi det er nært knyttet til antallet av mørke flekker på overflaten av solen.

Geomagnetiske induserte strømmer kan føre til utløsning av relevern med oversensitive sikkerhetsmarginer, som kan være ødeleggende for transformatoren. Dominoeffekter kan forekomme, noe som igjen kan føre til strømbrudd og tap av produksjon.

Utvikling av reduserende strategier og risikovurdering må gjennomføres. Viktige faktorer er prediksjon av romvær, modifikasjoner av kraftsystemet og beredskapsplaner.

Faktorer som påvirker geomagnetiske induserte strømverdier er også blitt vurdert, og gir et verktøy for å diskutere sannsynligheten for om et område er spesielt utsatt for kraftige geomagnetiske stormer eller ikke.

Det viste seg å være en utfordring å representere den geomagnetisk induserte strømmen ved hjelp av en spenningskilde. Dermed er resultater kun gitt for koblingsskjemaet hvor den geomagnetisk induserte strømmen er representert ved en likestrøm-

skilde koblet til den høyspentviklingen til den aktuelle transformatoren. Resultatene indikerer at en trefase trebent transformator er mindre utsatt for effekter knyttet til geomagnetisk induserte strømmer enn en trefase fembent transformator. Videre finner man at å ha en delta tertiærvikling gir høyere steady-state verdier i form av reaktivt effektforbruk og strømmer inn på høyspenningssiden av transformatoren. På den andre siden kan en observere at det reaktive effektforbruket og transformatorstrømmen har et mindre tidstrinn uten deltakobling. Følgelig, å ikke å ha en deltakobling resulterer i høyere reaktivt strømforbruk og transformatorstrøm til å begynne med. På grunnlag av resultatene konkluderes det med at trefase trebent transformatorer med en deltakobling synes å være det beste valget med tanke på sårbarheten mot geomagnetisk induserte strømmer.

Contents

Chapter 1

Introduction

1.1 Background

Solar storms pose a substantial risk to the power systems and thus a threat to humanity. Because of increasing complexity of the power system the effects of solar storms on power systems, especially relating to GICs, pose a serious threat with major consequences. If a GMS with magnitude in the range of the solar storm of 1859 would occur today it is estimated to cause billions of dollars of damage to technological systems, e.g. power grids and spacecraft electronics [Council, 2008].

Norway's Contingency Regulations impose on Statnett to mitigate risks associated with GMDs. This means primarily the mitigation of GICs induced by severe GMSs. No specific actions or use of technology are required [Beck, 2013], and Statnett has to perform risk analysis on the Norwegian power grid and investigate different mitigation strategies to find a good way to mitigate the GIC effects.

Power transformers experience numerous effects due to GIC flow through the high voltage winding, such as half-cycle saturation, which in turn can lead to transformer heating, harmonic generation and system voltage instability [NASA, 2013]. It may also lead to an increase of the transformer reactive power consumption.

The main objectives of the project realated to the providing of information was achieved reviewing articles about effects of GIC on power transformers. These articles were mostly selected from the database of IEEE, but also other project reports and articles were included.

The article Girgis and Vedante together with Chiesa et al., NERC [2013] and Lahtinen and Elovaara [2002] has been given extra attention as it discusses a wide range of GIC effects on power transformers. The article Girgis and Vedante claims that only some specific transformers could suffer some winding damage due to high winding circulating currents if exposed to high levels of GIC. It demonstrates that most power transformers would not experience much overheating or damage.

It is shown by Chiesa et al. that air path inductances play a signifiant role for reactive power consumption due to saturation of the outer limbs of three-phase five-legged power transformers. Chiesa et al. analyses the influence of transformer core topology and the air path inductances. The article is of special interest because it is considering a hybrid transformer model which is very similiar to the transformer models used in the Master's thesis. It is shown by Girgis and Vedante, Chiesa et al. and Lahtinen and Elovaara [2002] that the differential current harmonics due to GIC may cause maloperation of differential relays.

The document NERC [2013] addresses the transformer models that are available for GMD planning studies. They are divided into two categories: magnetic models describing reactive power consumption and harmonic generation caused by GIC and thermal models that account for hot spot heating due to GIC. This project will adress the reactive power consumption and harmonic generation of three-winding transformers under the influence of GIC.

The article Lahtinen and Elovaara [2002] provides test results for a 400 kV system transformer due to GIC occurences, and the test arrangements presented has served as inspiration for the circuit diagram used in this project.

In addition to the main topic of GIC effects on power transformers, the project report also provides an introduction to the background of the topic, i.e. literature review of articles related to solar storms, GICs and their effects on power systems. Articles used in the context of GICs and their effects on power systems were mainly selected from "IEEE Xplore Digital Library", and preferably journals and magazines published after year 2000. Information about the Sun and solar storms was primarily obtained from the website of NASA, being a recognized and credible independent agency of the United States government. Additionally, other papers that could provide a better understanding of the topics were used with a critical eye.

The GIC effects on power transformers need further investigation to better understand how they respond to GIC, and thus be better prepared to mitigate the GIC effects due to big GMDs, both in terms of an economic and safety aspects. Moreover, to do so, one should have some basic knowledge of solar storms, GIC and their effects on power systems.

The main objectives of this Master's project are

1. Provide basic knowledge of solar storms, geomagnetic induced currents and their effects on power systems

2. Gather information about GIC effects on power transformers

3. Construct a simple circuit diagram of part of a power grid in ATPDraw

4. Investigate how the GIC effects are influenced by some specific conditions:

    - Three-phase three-legged and three-phase five-legged transformers
    - With or without a delta connected tertiary winding (Δ) in the transformer
    - Magnitude of air path inductances
    - Magnitude of the geomagnetically induced electric field
    - Magnitude of GIC
    - Investigate if the X/R ratio, especially with respect to the zero sequence system, in the adjacent high voltage lines along with the power transformer is crucial for the time to equilibrium of the GIC in the power transformer.

5. Evaluate the constructed circuit diagrams and the different power transformer designs, and give recommendations regarding which power transformers to prefer.

1.2 Limitations

Two electrical circuit models, which are suppossed to represent a section of a power grid, are presented, where only the results from one of the models are included in this project report. The selected model is highly simplified, e.i. the HV windings of the power transformers are connected at the same node and the GIC is represented by a fixed DC current flowing into one of the HV windings.

Parameters chosen for the simulations, e.i. GIC value and air path inductance, are selected on the basis of related articles and by intuition. For some unknown reason the simulation model has difficulty dealing with small values of the air path inductance, thus it is never set to a value below 250 mH. And, the size of the time step value in ATPDraw is limited, which may cause inaccurate results.

Due to shortage of time there were only performed data simulations, while the ideal would have been to verify the results with a real GIC setup in a power electrical laboratory. Thus, because of lack of data for comparison, when analyzing the results the aim is to find patterns and trends rather than exact numerical results.

1.3 Approach

A theoretical bakcground of the topic was provided by conductiong a literature review. Furthermore, the main objectives concerning the investigation of GIC effects on power transformers were completet by using the ATPDraw program. Simulations are done separately for 300 MVA three phase three-legged transformers and 300 MVA three-phase five-legged transformer. The results are analyzed with respect to several measurements: the reactive power consumption, magnitude and current harmonics of the transformer where the GIC is applied, and the flux distribution in the core, limbs and yokes as well as air paths. The tasks related to Δ, the magnitude of air path inductances and the GIC magnitude are carried out in a similar manner.

1.4 Structure of the Report

The rest of the report is organized as follows. Chapter 2 gives an introduction to solar storms and GIC. Chapter 3 gives a theoretical and historical background of the influence of GIC on power transformers and power systems. Chapter 4 mainly describes the circuit diagrams developed in ATPDraw, as well as the transformer models used in this project. Chapter 4 also gives a description of measurement methods. The simulation results from ATPDraw is given in chapter 5 and Appendices B-E. Chapter 6 gives a summary, a discussion of the results and recommendaions for further work.

Chapter 2

From Solar Storms to GIC

The solar activity on the Sun is the cause of most of the terrestrial space weather and, with the possible exception of a nova shockwave, it is normally the only natural source of GICs that is taken into consideration [Thorberg, 2012].

In this chapter the chain of events leading to GIC will be reviewed, beginning at the Sun and ending up as a current flowing through the power system.

2.1 Solar Storm

Figure 2.1 illustrates a solar storm. Solar wind is a constant stream of charged particles emitted by the Sun, which in case of facing Earth are deflected by the Earth's magnetic field, the magnetosphere. This magnetic interaction is observed at the sunward side of the Earth as compressed field lines, leading the field lines to snap and reconnect. Now the magnetosphere and the magnetic field of the solar wind are linked and holes are created at the north pole and the south pole, letting the charged particles from the solar wind enter the magnetosphere. The solar wind continues its way past the Earth and the linked field lines of the magnetic field on the side of the magnetosphere facing away from the Sun are stretched.

Due to Len'z law the interaction of the solar wind with the Earth's magnetic field causes a current to flow in the ionosphere. This current is known as an electrojet and

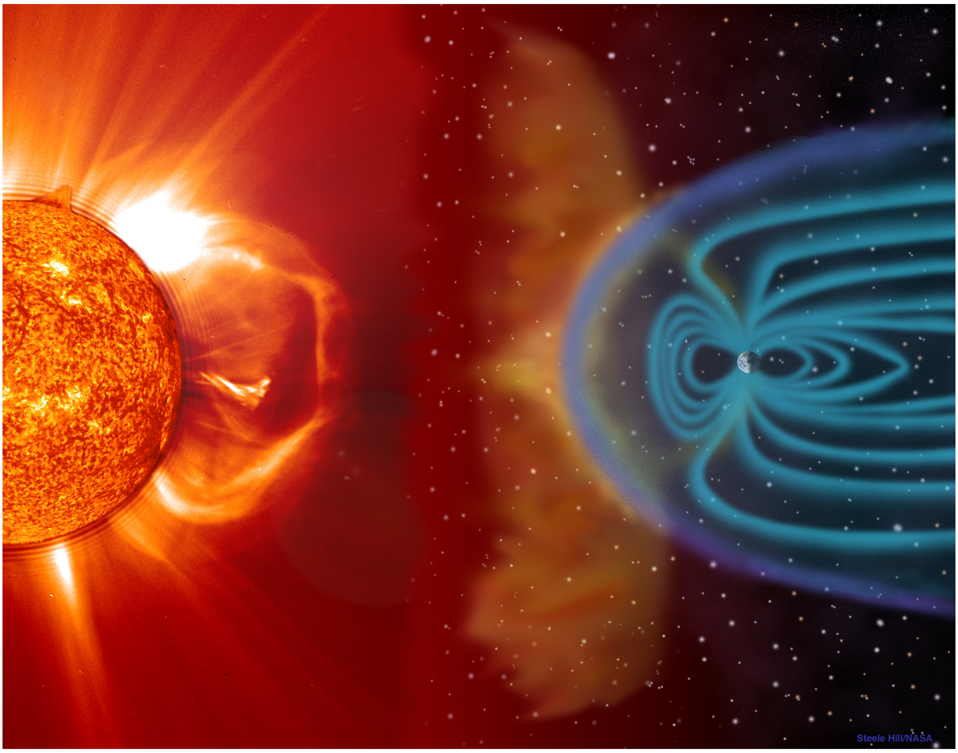

Figure 2.1: The illustration demonstrates a coronal mass ejection traveling through space and its interaction with the Earth's magnetosphere [Hill/NASA] (Courtesy of Steele Hill/NASA).

can reach several millions of Amperes[Thorberg, 2012]. Figure 2.1 also indicates the fact that the GIC levels are affected by the Earth's axial tilt and the season of the year [Thorberg, 2012].

Explained in simple terms, most of the time the solar wind is too weak to penetrate the magnetosphere. But in some cases, e.g. in the case of a coronal mass ejection (CME), the magnetic field from the charged particles of the solar wind may be strong enough for the charged particles to get inside the magnetosphere.

2.2 Sunspots and The Sunspot Cycle

On the photosphere, which is the definition of the surface of the Sun, it can be observed groups of dark spots. These dark spots are called sunspots and are temporarily, during from a few days to a few months. Sunspots can be seen with the naked eye, and are observed as dark compared to the surrounding areas because of the low temperature compared to the rest of the photosphere. The reduced temperature at the sunspots is due to high magnetic fields that counteract the convection preventing hotter material to reach the surface.

The number of sunspots varies with a cycle of 11 years, which is approximately the time the Sun uses to change polarity. This phenomenon is called the sunspot cycle or the solar cycle. One 11-year cycle is defined as the time between the minimum occurrence of sunspots with changed magnetic polarity. The current solar cycle is the solar cycle 24, being the 24th solar cycle since 1755. The periodicity of the sunspot cycle is shown in Figure 2.2.

The number of sunspots is strongly related to CMEs, which is the cause of GICs. It is also an indication of creation of other space weather phenomena such as solar flares and solar proton events (SPE). So, counting of sunspots is still an easy and excellent way to measure the activity of the Sun, even though today there are several modern ways to measure the solar activity.

2.3 Some Space Weather Phenomena

Solar flares, CME and solar proton events (SPEs) are only three of the phenomena that occurs during solar storms, but are the predominant causes to adverse effects at the ground level and in vicinity of the Earth (see Table 2.2). GICs and GMS mainly arise from CMEs.

The solar storm events have different arrival times, i.e. amount of time spent from the sun to Earth, and effect duration (see Table 2.1).

2.3.1 Solar Flare

Explosions as a result of built up magnetic energy in the solar atmosphere leads to solar flares, and heat up particles, e.g. electrons, protons and heavy nuclei which are accelerated in the atmosphere of the Sun. The radiation represents the entire electromagnetic spectrum, from radio waves to gamma rays.

Immense amounts of energy are released, and the energy released from a large solar flare is equal to the sum of the energy released from ten million volcanic explosions at the same time[NASA, d].

2.3.2 CME

Similar to solar flares, CMEs occur from massive explosions of energy at the Sun, where CMEs are nearly always correlated with the strongest flares. In spite of the common cause and the fact that both solar storm phenomena may occur at the same time, solar flares and CME are considered as separate phenomena due to their different properties, e.g. appearance, traveling time and effects near planets [NASA, a].

The CME can be compared to the cannonball when firing a cannon, the cannonball being a gigantic cloud of magnetized particles ejected from the Sun moving in a certain direction, i.e. CME, while the flare would represent the muzzle flash [NASA, a].

2.3.3 SPE

SPE occurs from either a flare or a CME. It is a result of an acceleration of particles, primarily protons, emitted by the Sun.

Table 2.1: Arrival Time and Effect Duration for the most important Solar Storm Events [Marusek, 2007].

Event	**Arrival Time**	**Effect Duration**
Solar Flares	8 minutes	1-2 hours
Solar Proton Event	15 minutes to a few hours	Days
Coronal Mass Ejection	2-4 days	Days

Table 2.2: Solar Storm Threats [Marusek, 2007].

Threat	Solar Flare	Solar Proton Event	Coronal Mass Ejection
Induced Currents			X
Geomagnetic Field Distortions		X	X
Nuclear Radiation Exposure		X	X
Ionospheric Reflectivity and Scintillation	X	X	X
Other Atmospheric Effects			
- Aurora Borealis			X
- Atmospheric Envelope Expansion	X		X
- Shifting Radiation Belts			X
- Ozone Layer Depletion		X	

2.4 GICs

2.4.1 The Causal Factors Associated with GICs

Sunspots can give rise to solar flares and CMEs. A CME has its own current and magnetic field which are strong enough to interfere with the Earth's magnetic field. That is, the CME leads to large fluctuations of the currents in the magnetosphere and the ionosphere, causing electrojets. The disturbances of the earth's geomagnetic field due to the electrojets induce a geoelectric field at the Earth's surface. This field will induce a quasi-DC voltage in technological conductor networks. If these conductors are parts of a closed loop, e.g. neutral grounding of transformers at the ends of a high-voltage transmission line, a quasi-DC current will circulate by entering and exiting the power system through the neutral grounding of transformers, see Figure 2.3. This current is known as geomagnetic induced currents (GICs) and has a range of frequency between 0.1 mHz-0.1 Hz, which is equivalent to waves with periods ranging from seconds to a few hours.

The duration of a GMS may be one to two days and the fluctuations of the geomagnetic field will continually generate GICs with a varying intensity. Most of the time the GIC level will be low to moderate, whereas high GIC pulses are only generated sporadically [NASA, 2013].

GIC is only one of many effects that have their roots in space weather driven by solar activity, but may have one of the most destructive impacts on humanity as it affects electric power transmission grids, oil and gas pipelines, telecommunication cables and railway circuits [Myllys et al., 2014].

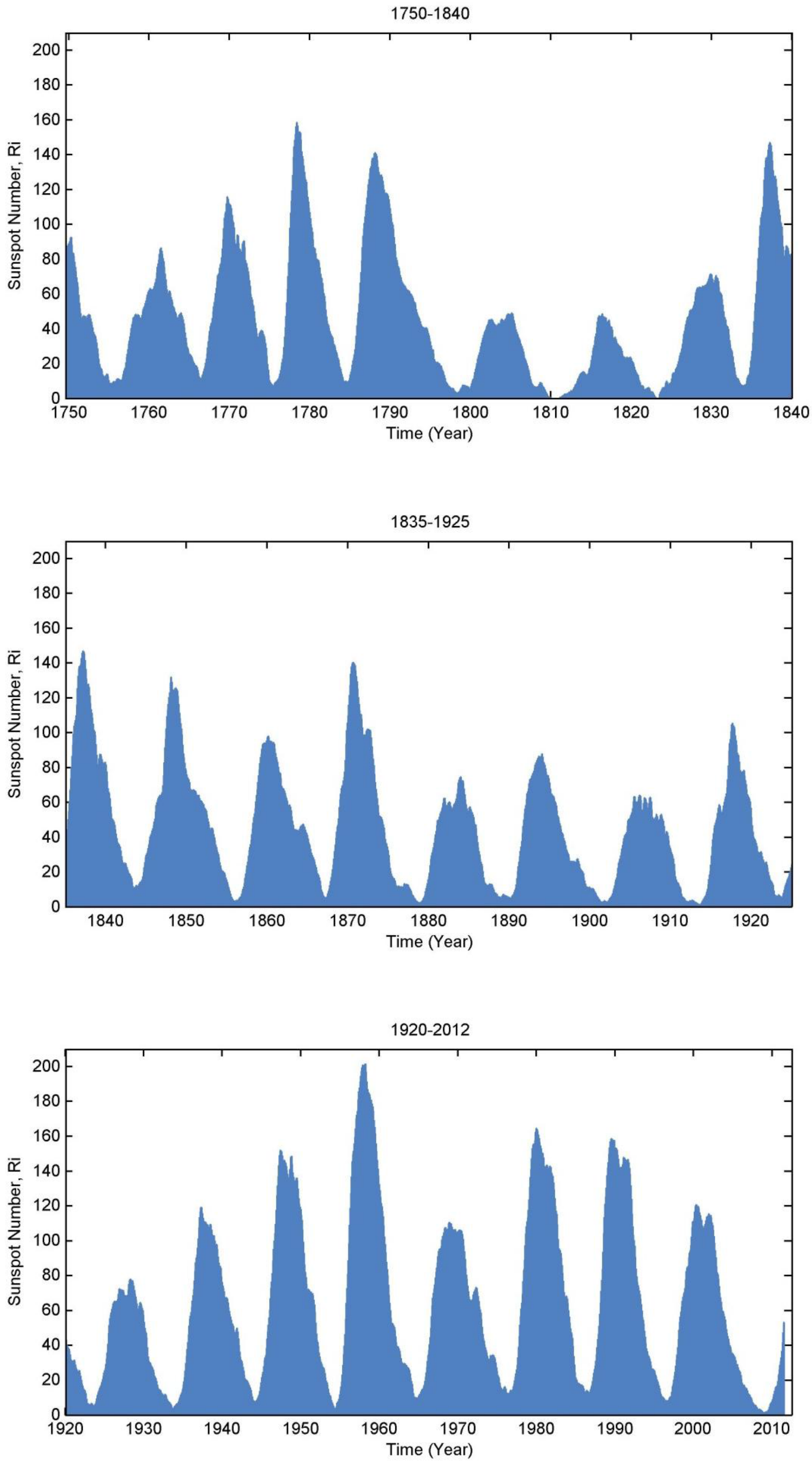

Figure 2.2: Sunspot cycles from 1750 to 2012 [Thorberg, 2012] (data courtesy SIDC-team).

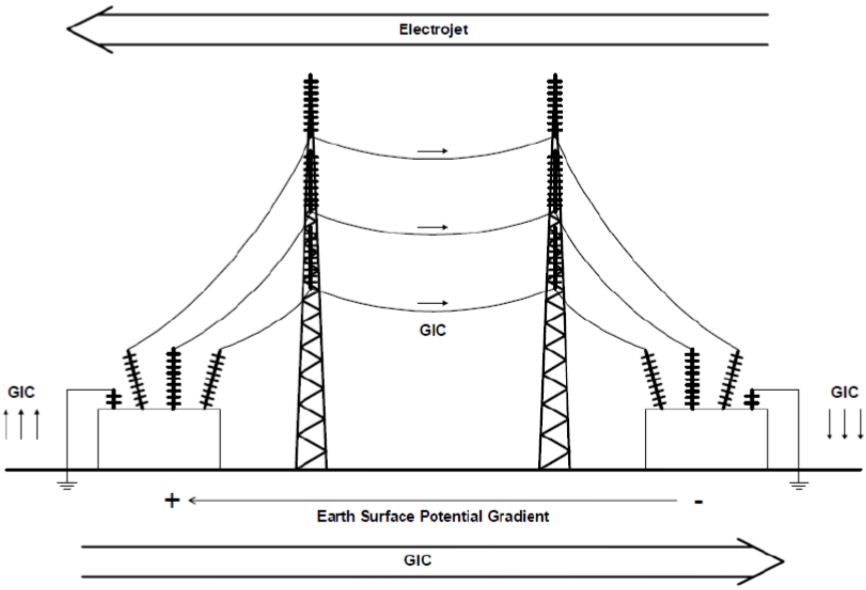

Figure 2.3: Illustration of GIC generation in power network [Thorberg, 2012].

Chapter 3

Effects of GICs on Power Transformers and Power Systems

Many technological conductor networks, e.g. telecommunication cables, railway circuits, oil and gas pipelines, suffers from GIC problems.

This chapter will, in accordance with the main objective of this project paper, give an overview of the GIC effects on the electric power systems, with primary focus on the effects on the transformer.

It can easily be seen from Figure 3.1 that the effects from GICs on transformers are many and that the transformer is a crucial component with regard to understand how the power system respond to solar storms and how to mitigate the GIC effects.

There are other components in the power grid that are affected by GICs, e.g. generators, high voltage synchronous motors and protection relays , but a detailed description of the GIC effects of these is beyond the scope of this project. Nonetheless, because of the interdependencies between the components in the power grid, it is important to investigate the GIC response of all components to be able to understand and predict the consequences of GICs.

Still, a short description of possible relay protection failure under the influence of GICs will be given due to its importance: Poorly adjusted protection schemes may lead to false trips which can cause cascading failures and black out. This is what happened under the Hydro-Québec event.

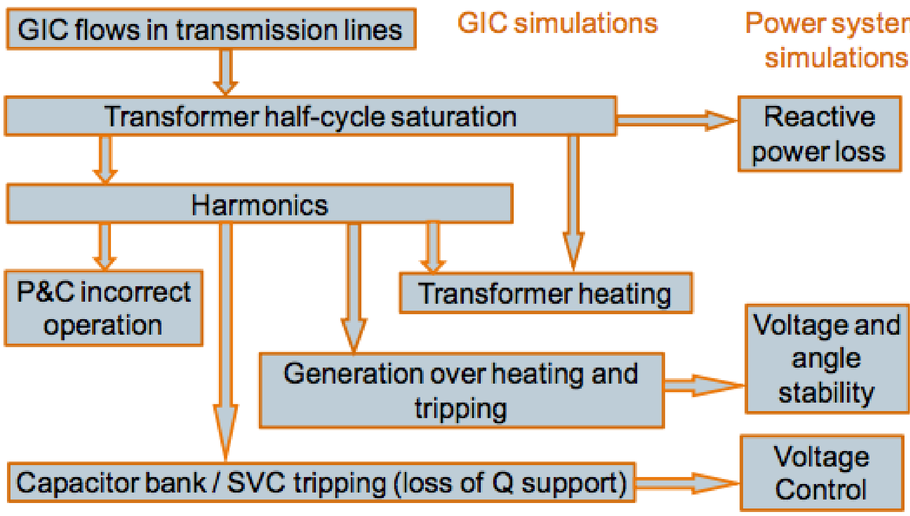

Figure 3.1: Potential effects of GICs on power system grid [AG].

3.1 Historical Events

There have been many strong GMSs leading to critical GIC levels, and there are still many to come. In this section three historical events which are of special importance will be presented. The first is the largest GMS ever recorded, the second resulted in a severe power blackout and the third gives clear indications that Norway could be vulnerable to GIC events.

3.1.1 The Carrington Event (1859)

The largest GMS ever recorded occurred on the morning of September 1, 1859. It is referred to as the Carrington event after the British astronomer Richard Carrington which, for the very first time in the history, observed a solar flare. While a CME normally spends two to four days (see Table 2.1) on its journey from the Sun to the Earth, it took 17 hours before the Earth experienced a big GMS, probably due to a large CME. It lasted for days and the effects where many and widespread. Colorful northern lights could be observed all over the world at latitudes as far south as Tahiti, and it is reported that light emitted from the northern lights was bright enough to read the newspaper without any further light sources. The GMS also caused global telegraph lines to spark, setting fire to some telegraph offices and telegraph systems all over North America and Europe went down [Baker et al., 2008].

The Carrington event is the largest GMS in the last 500 years. From sunspot records and samples from ice cores scientists assume that GMSs of similar magnitudes are to be expected once every 500 years, or even as often as once in a century. Even though it may occur a GMS with a magnitude greater than the one experienced during the Carrington event, research and development related to worst case scenarios are based on the Carrington Event.

It is important to emphasize that both the solar cycle of 11 years and the assumption that a GMS of magnitude in the range of the one during the Carrington event will occur once every 500 years arise only from statistics. Which means they give no more than probabilities of a massive CME hitting Earth. However, a severe GMS scenario leading to large GICs can occur at any time, and preparation against an estimated worst case scenario should be carried out as soon as possible.

3.1.2 The Hydro-Québec Event (1989)

On the night of March 13, 1989 a severe GMS caused a protective relay to trip due to GIC, which in turn made a 100 ton static VAR capacitor trip. This led to tripping of several protective relays, cascading failure, and resulted in the entire Quebec power grid to collapse. The whole sequence of failure events happened fast and within 75 seconds from the first capacitor tripped [Thorberg, 2012] six million people where left without power for up to nine hours during this wintry period.

After the Hydro-Québec the world realized the seriousness of the imposed GIC risk and several power companies in the Western world began to investigate GIC risk and do research on mitigation strategies.

3.1.3 The Halloween Storm (2003)

At the end of october and the beginning of november 2003 several CMEs hit earth in a cumulative manner and caused severe GMSs. The sequence of storms due to solar flares and CMEs during this period is known as the Halloween storm.

Once again a blackout occurred and 50 000 people connected to the power grid of Malmö were left without power for 20-50 minutes. The blackout was caused by the high geoelectric field values of 2 V/km saturating a transformer due to GIC, which in turn tripped a relay that was too sensitive to the third harmonics[Thorberg, 2012].

South Africa was also affected by the Halloween storm and several large transformers were damaged. But the lack of measuring equipment makes it hard to analyze the events retrospectively.

The Halloween storm also had major consequences for different technological systems, e.g. communication and navigation systems.

3.1.4 Norway

Until today, Norway has not uncovered any serious or widespread system damage to be caused by GMDs. But still there are some incidents worth mentioning, such as the activation of a 90 MVAR shunt capacitor at Kristiansand in 1999, caused by GIC flows. Another example happened at Lyse in 2004 where a Buchholz relay tripped and led to disconnection of a transformer [Beck, 2013].

3.2 Exposed Areas

3.2.1 Geomagnetic Latitude and Magnitude of GMS

Geomagnetic Latitude

The geomagnetic field that surrounds the earth is working like a solar storm shield and thus the GICs are dependent on the geomagnetic latitude (GML). For the same reasons as the northern lights, which also originate from electrojets, are more frequent and much brighter in northern regions, the GICs are in general more frequent and stronger at high latitudes.

For most strong GMSs it seems to be a threshold around 50-55 degrees of GML, with a drop of the geoelectric field amplitude of around a factor of 10 from 60 to 40 degrees [Thorberg, 2012]. Then it is not surprising that two of the most important GIC-events took place in Canada and Sweden as they are situated above the threshold. Yet there are examples of GIC-effects much farther south, e.g. vibration and noise in transformers at the Shanghe substation and the Ling'ao nuclear power plant in China were experienced due to GICs [Liu et al., 2009]. The Shanghe substation and the Ling'ao nuclear power plant have a GML of approximately 30 and 20 degrees, respectively. Thus, together with the GIC impact from the Halloween storm on South Africa, with a GML of about -40 degrees, it proves that the threshold around 50-55 degrees is only indicative.

In theory, given the same assumptions in terms of electrojet and latitude, the GIC-level should be equal in both south and north relative to the GML. But in reality far south in the Southern Hemisphere there is mostly sea, thus GIC problems in this region will not be as widespread as in the Northern Hemisphere. The main areas included in the region below GML -40 degrees are the tips of Chile, Argentina, part of South Africa and Australia, Arctic and New Zealand.

Inside the aurora oval the geomagnetic field is directly linked to the solar wind. During a solar storm it will be observed strong GMDs within the aurora oval, but the influence on these GMDs will mostly be controlled by the parameters in the solar wind, i.e. velocity, magnetic field and density. While in the aurora oval the GMDs is determined by the dynamics of the magnetosphere, which is loaded with energy from the solar wind.

Magnitude of GMS

Under big GMDs due to big GMSs the aurora oval will be extended. The expansion of the aurora oval consists mostly of the southern boundary to move even further south. The northern boundary, on the other hand, will move further south somewhat, but not as much as the southern boundary. That is, under great GMSs all of Norway will be covered by the aurora oval, and the biggest GIC values are still most likely to be found at high magnetic latitudes. But one must still consider other parameters such as ground conductivity, coast lines and configuration of the power grid, which all have an impact on the GIC susceptibility, and may make other areas more vulnerable.

It is suggested that even small magnitudes of GIC over an extended period of time could lead to transformer failures[Gaunt, 2014]. Thus, it may be that small GMSs, which happens with a higher frequency than the strongest GMSs, could be part of the problem for several failures in the power system without having been detected as one of the causes. If that is the case, GICs are of greater importance than assumed and risk assessment and development of mitigation methods due to GICs should also include low GIC values.

3.2.2 Ground Conductivity and Conductance Maps

Ground Conductivity

Countries normally related to GIC events are typically countries in the north, e.g. Canada and Sweden. Also, Norway is located far north and should therefore be particularly vulnerable to GIC events. An interesting fact is that because of the smaller values of ground conductivity in the south of Norway, which leads to an increase of the electric field, magnitudes of GICs which occurs south in Norway are comparable to the magnitudes which are expected to occur in the north during extreme GMSs. And more important the highest GICs will probably occur in the south of Norway because of the structure of the power grid. While in the north significantly GIC levels will only occur in proximity of the main transmission line [Myllys et al., 2014].

Conductance Maps

A map in cells on the electrical resistivity distribution in Europe has been developed [Ádám et al., 2013]. The GMD may manifest itself as far as 100 km beneath the surface of the Earth and conductance maps are developed, i.e. Figure 3.3, both for the upper 80 km and the upper 160 km of the Earth. These maps are of great importance in simulations of GIC-related risk endangering the power grids and communications systems [Ádám et al., 2013]. But the cells are big and the accuracy of the simulations are limited. Further development of the conductance map is desirable to get more accurate simulations of GIC flow in Europe.

3.2.3 Coast Effect

The change in surface conductivity due to the ocean-land interface may enhance the geomagnetically induced electric field on land close to the ocean. This phenomenon is called the coast effect and depends on the land and sea conductivity, the depth of the sea and the geomagnetic field characteristics [NERC, 2013]. The coast effect is unfortunate because electrical generating plants tend to be placed near the seashore for cooling purposes[Gilbert].

In the transition from sea to land the horizontal conductivity structure experience a great change as shown in Figure 3.2. Because the conductivity is higher in the seawater than in the soil, higher currents are induced i the sea than in the crust of the earth. When a current is crossing the boundary between land and sea the geoelectric field perpendicular to the boundary is higher when taking into account the coast effect than only considering the land conductivity. This arises from the necessity of current continuity while the charge cannot accumulate and there is a difference between the current density arriving at the coast from the sea and the one departing from the coast into the land [NERC, 2013].

The physics behind the coast effect is quite complex and a further description is out of scope for this report, and the coast effect on transformers will not be looked into in this project. Nevertheless, Norway has a long coastline and it would be natural to look into the impact of the coast effect when simulating GIC-scenarios in the Norwegian power grid.

3.2.4 Length

The vulnerability of power transmission lines increases with the length of the line. The basis for calculating the voltage across a section of a conductor is given by Equation 3.1,

$$V_{AB} = \int_A^B E \cdot \mathrm{d}l, \tag{3.1}$$

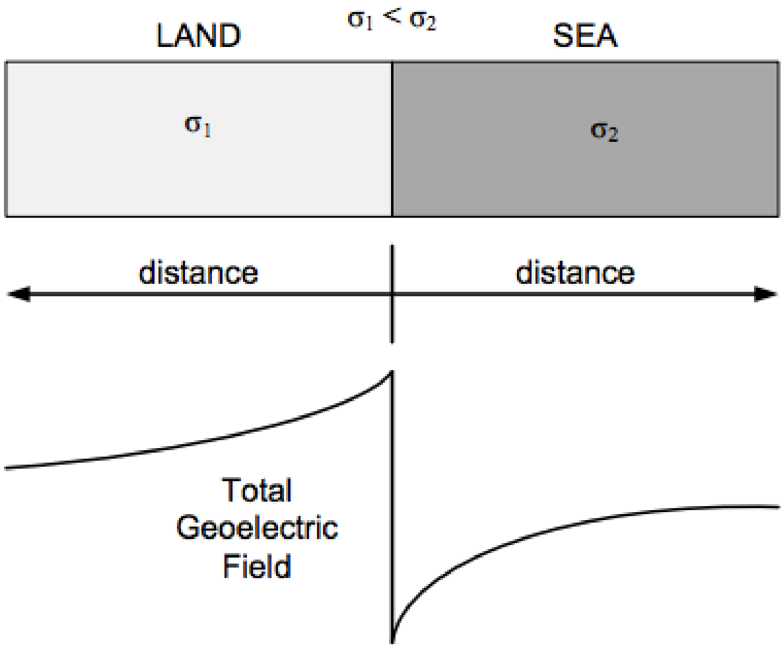

Figure 3.2: Coast effect [NERC, 2013].

where V_{AB} is the voltage between nodes A and B induced by the electric field E over a line segment, e.g. a transmission line. If the electric field E across the power system is assumed to be uniform the voltage across transmission lines could be found be integrating over straight lines between substations [Bernabeu, 2013].

3.2.5 Orientation

The gradients of earth surface potential are larger in the east-west direction than in the north-south direction. Thus, the susceptibility to GICs of a power line is influenced by the orientation of the line, oriented in the east-west direction being the least favorable [Marusek, 2007].

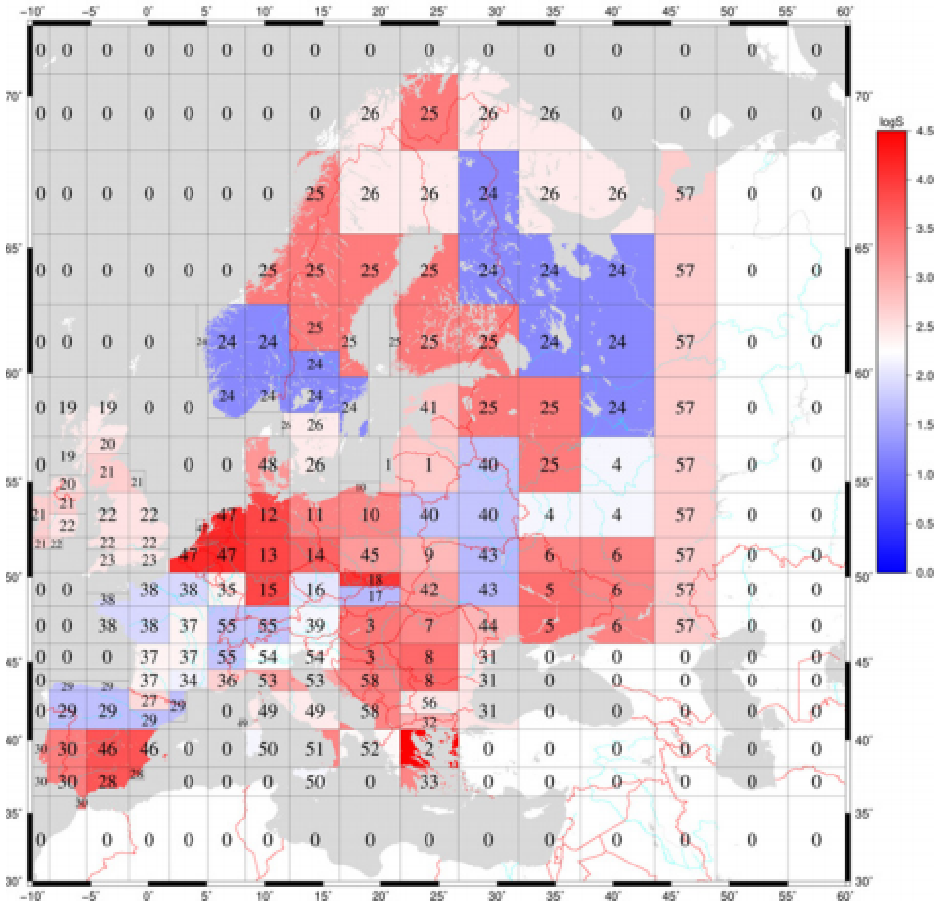

Figure 3.3: Conductance map of Europe, upper 80 km [Ádám et al., 2013].

3.3 Transformers

GICs may flow through any grounded component of the power grid. But of all the consequences that may occur in the power grids due to solar storms, the consequences of GIC flowing through high voltage transformers are maybe the most severe ones and pose the greatest risk. It can cause damage to transformers and lead to blackouts, where both consequences will result in great financial expenses and may even endanger human lives. Therefore the effects of the GIC on the transformers should be carefully examined and thoroughly understood to avoid such incidents.

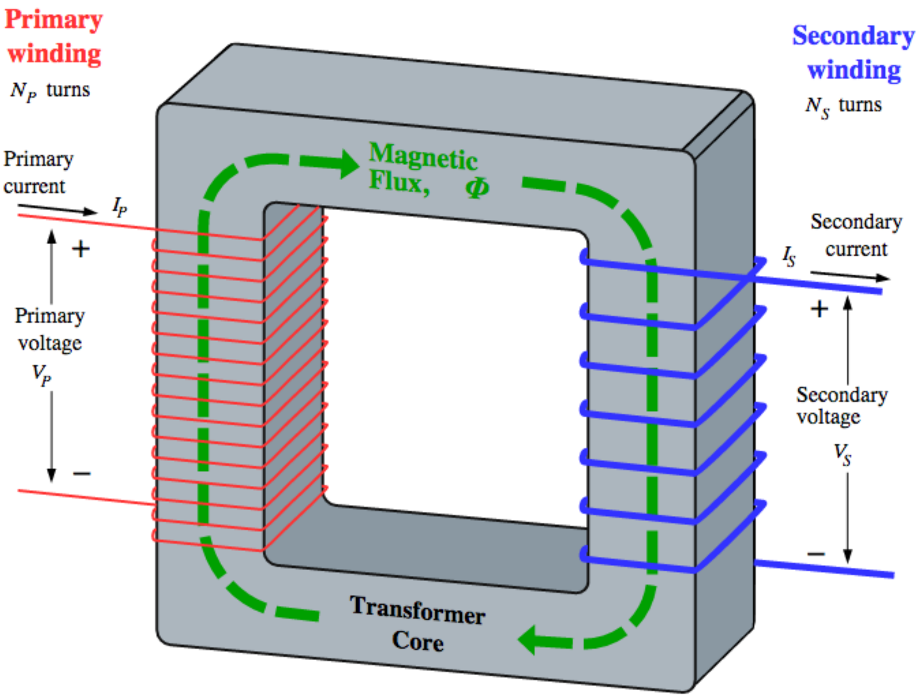

Figure 3.4: Idealized single-phase transformer [BillC].

3.3.1 The Concept

GICs will flow through the high voltage transformers. In power transformers this causes half-cycle saturation, which in turn can lead to transformer heating, harmonic generation and system voltage instability [NASA, 2013]. It can also lead to an increase of the reactive power consumption.

3.3.2 Half-Cycle Saturation

When GICs, which are quasi-DC currents, flows in a power transformer, it causes a unidirectional DC flux to flow in the core. As a result the total flux in the core is the sum of the DC flux and the AC flux, as shown in Equation 3.2. Consequently, in the negative half-cycle the DC flux will be subtracted from the AC flux and there is no saturation. While in the positive half-cycle the core will go into saturation due to the DC flux, as shown in Figure 3.6, hence the name half-cycle saturation.

$$\phi = \phi_{AC} + \phi_{DC} \tag{3.2}$$

The magnitude of the DC flux depends on three factors: the magnitude of the induced quasi-DC current, number of turns in the windings where the quasi-DC current flows, and the reluctance of the path of the DC flux [Girgis and Vedante]. This relation is shown in Equation 3.3,

$$\phi_{DC} = \frac{N \cdot \text{GIC}}{\Re}, \tag{3.3}$$

where N is the number of turns, GIC is the magnitude of the DC current and $\Re$ is the reluctance of the magnetic circuit. The reluctance $\Re$ is found using Equation 3.4,

$$\Re = \frac{l}{\mu \cdot A}, \tag{3.4}$$

where l is the length of the magnetic circuit, μ is the permeability of the material and A is the cross-sectional area of the circuit. Furthermore the reluctance $\Re$ is a function of the ac excitation. So, to find the magnitude of the direct flux bias ϕ_{DC} one has to take into account the direct flux bias ϕ_{DC} dependency of the ac excitation and the level of saturation, and not only the GIC magnitude [Bernabeu, 2015].

The significant increase of reactive power consumption due to half-cycle saturation can cause unusual transmission flow of active and reactive power, generator problems due to reactive power limits, and intolerable system voltage depression [Fuchs and Masoum, 2008].

3.3.3 Thermal Effects

GIC flowing in the transformer leads to a higher magnetizing current, which shape produce a higher leakage flux, that also contains a lot of harmonics. This leads to a significant increase of eddy and circulating current losses in both windings and structural parts of the transformer, causing heat generation and transformer losses [Girgis and Vedante]. Because the GIC-imposed thermal duty is outside the standard service parameters the increase in temperature and load losses of windings and structural parts

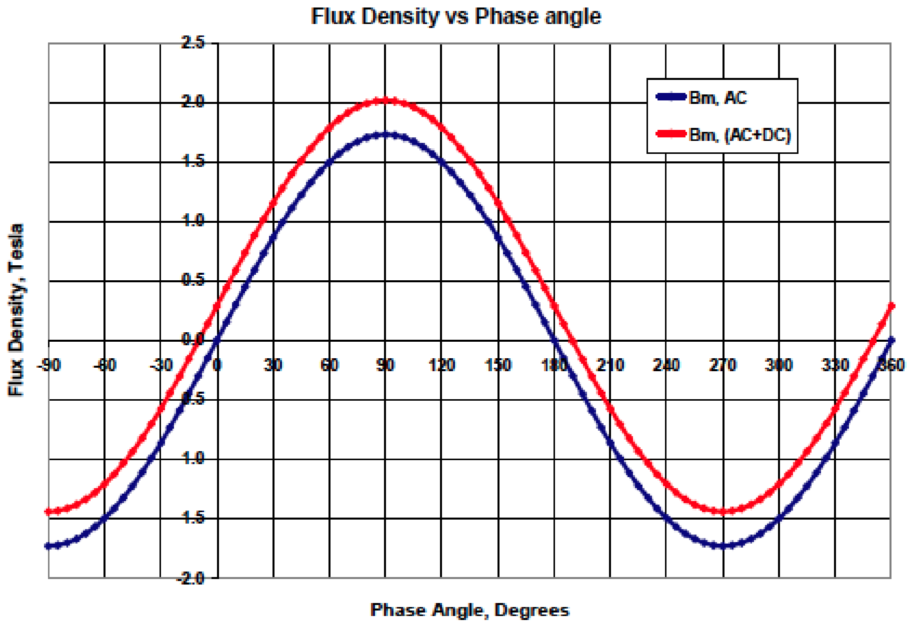

Figure 3.5: Flux density shift in the core caused by DC [Girgis and Vedante].

should be assessed individually for each type of power transformer design [NASA, 2013].

Several articles from the "IEEE Xplore Digital Library", e.g. [Girgis and Vedante] and [NASA, 2013], concludes that overheating due to induced DC-current should not necessarily have any negative impact on the reliability of the transformer. The reason is said to be that the duration and frequency of the occurrence of GICs is too short to produce a critical temperature rise and low enough to give the transformer time to cool off, respectively.

The article [Girgis and Vedante] concludes that in most cases even high levels of GIC should not lead to damaging overheating of neither windings nor structural parts of power transformers, with core form and shell form being the exceptions. It claims that some cases of significant overheating and winding damage believed to be caused by GICs, were found to be caused by other effects, or by system instability experienced during a GIC event [Girgis and Vedante]. The article [NASA, 2013] confirms the necessity to determine the possibility of winding overheating due to high levels of GIC, but depreciate the overheating of the tank wall as an issue.

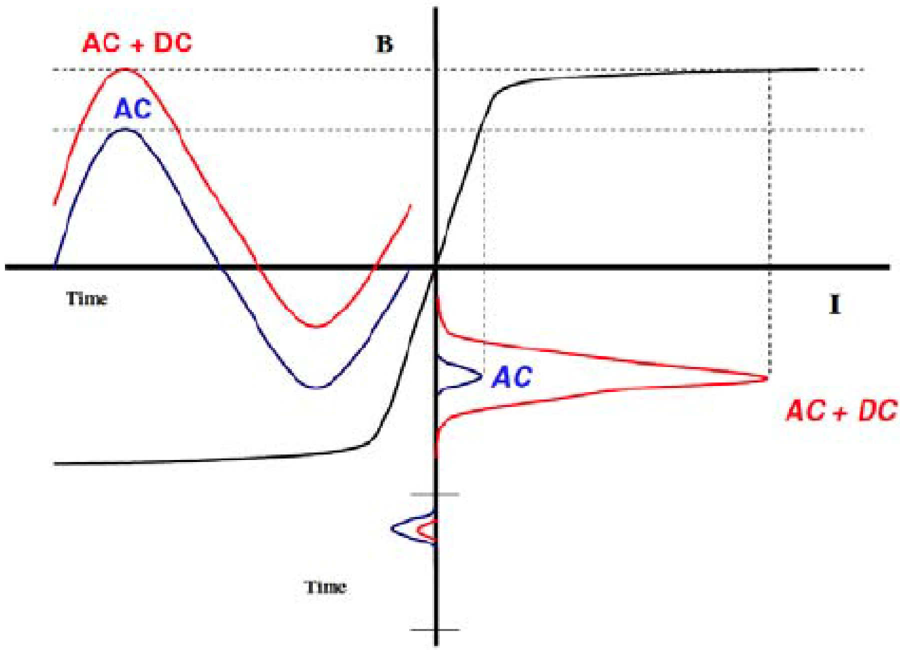

Figure 3.6: Part-Cycle, Semi-Saturation of Transformer cores [Girgis and Vedante].

In the research on whether the Norwegian power grid is exposed to solar storms, Statnett wants to measure the temperature in transformers, at points where it is most likely to experience high temperatures due to GICs. In this way one can find the degree of the correlation between overheating damaging and GIC flow.

3.3.4 Dependency of Type of Transformer

The magnitude of the DC flux shift in the core is dependent on the magnetic reluctance of the DC flux path [Girgis and Vedante], hence the extension of GIC effects on power transformers depends on the design of the core.

In Figure 3.7 the white arrows symbolize the possible return paths for induced DC flux and the larger gray arrows symbolize the induction of magnetic flux from the windings. The core designs with return paths through the limbs are more likely to saturate from GICs. So, although the three-legged core and the five-legged core will conduct the same amount of GICs, the three-legged core will not saturate as easily [Thorberg, 2012].

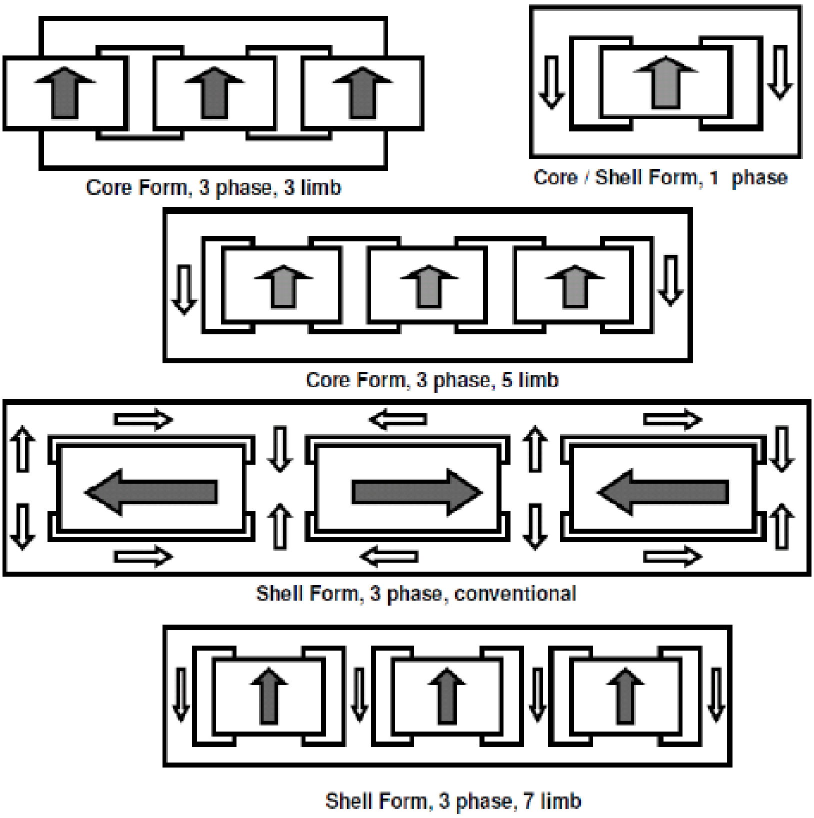

Figure 3.7: Core DC Flux path in various core types [Girgis and Vedante].

For the three-phase three-legged core the return path of the DC flux begins at the top yoke, continuing through the high reluctance path to the tank cover, going through the tank wall, returning to the bottom yoke through the high reluctance path from the tank bottom. This results in the highest reluctance path of the transformer types which gives the smallest DC flux shift. Thus the three-phase three-legged core is the least sensitive to GICs [Girgis and Vedante], while the single-phase transformer on the other hand is more sensitive than three-phase transformers.

The different DC flux shift experienced from GICs in different core types leads to varying magnitudes of magnetizing currents drawn by the transformer. In this context, transformers may be divided into two groups: three-phase three-legged transformers and other core types. In Figure 3.8 these groups are represented by a large three-phase three-legged transformer and a large single-phase transformer, respectively. It can also be seen in Figure 3.8 that the magnetizing current drawn by the single-phase transformer is much higher than the magnetizing current drawn by the three-phase transformer for the same values of DC currents flowing in each phase [Girgis and Vedante]. Also, since the return limbs is much less than the sum of the main limbs for the group represented by the large single-phase transformer, saturation will occur at an earlier time than for the three-legged transformer [Price, 2002].

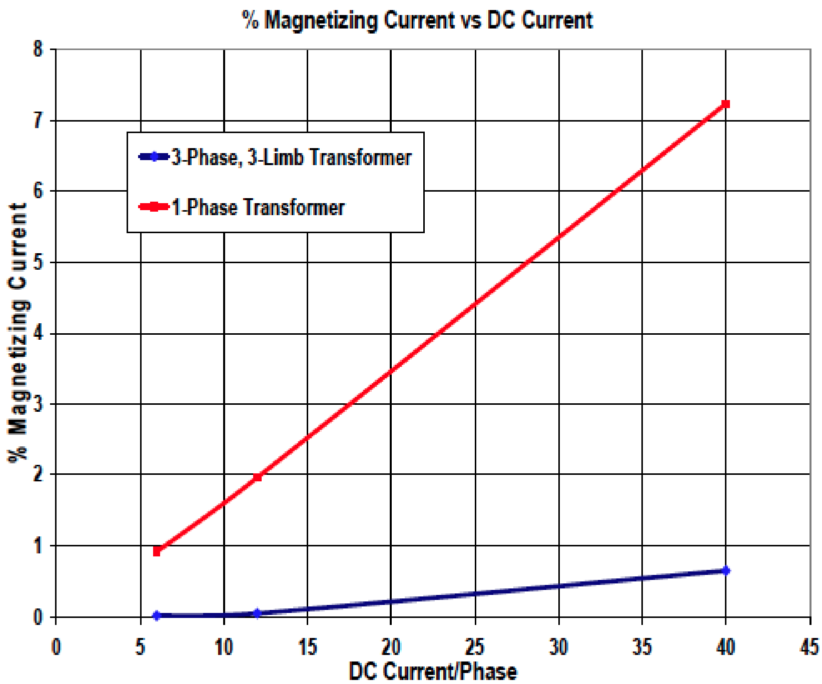

Figure 3.8: Peak magnetizing current for 2 different core types [Girgis and Vedante].

Earlier the manufacturer has not been required to provide knowledge of transformer functionality and sensitivity against GICs. Today the specification of GIC tolerance levels for new transformers is usually included in the datasheet of the transformer. A further development of this trend should be encouraged so that the buyer can make a reasonable choice of transformer considering the risks associated with GICs.

3.3.5 Δ

In Figure 3.9 one can see that the dc equivalent circuit of both two-winding and three-winding transformers are the same. This is because the Δ does not provide a path for GIC flow in steady-state and is therefore not included [NERC, 2013]. H1, H2, H3, L1, L2 and L3 represents the nodes of the three phases on the HV and LV side. H0 and L0 represent the neutral winding. Both H0 and L0 may be ungrounded, but if the GIC effects are to be studied at least the H0 need to be grounded. RWH1 and RWL2 refer to the DC winding resistance of the HV side and the LV side, respectively.

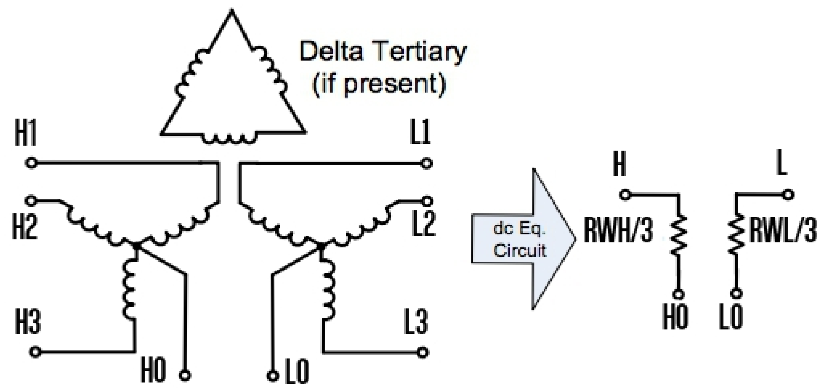

Figure 3.9: Single-phase dc equivalent of a two-winding or three-winding transformer [NERC, 2013].

Applying a DC step voltage to the HV winding may cause a current flow in the Δ if the transformer is unsaturated. But when reaching the point of saturation the applied DC voltage will cause the induced GIC in the tertiary winding to fall to zero. Additionally, the delta connection will work as a path for the triplen harmonics [Price, 2002].

3.4 Power Systems

3.4.1 Harmonic Generation

Saturation in the power transformer caused by GICs leads to induced harmonic currents. The effects due to these harmonics are many, some of them are given in the list below [Fuchs and Masoum, 2008]:

- Overheating of capacitor banks
- Possible misoperation of relays
- Sustained overvoltages on long-line energization
- Higher secondary arc currents during single-pole switching
- Higher circuit breaker recovery voltage
- Overloading of harmonic filters of high voltage DC (HVDC) converter terminals
- Distortion of the AC voltage wave shape that may result in loss of power transmission

Some particularly important issues are the increase of reactive power consumption and the probability of misoperation of protection and relay schemes when the configuration of these are not taking into account the harmonic currents produced by GICs.

Figure 3.10 shows the % harmonic content of two types of transformers, in accordance with the group division explained in subsection 3.3.4. It can be seen in Figure 3.10 that three-phase transformer subjected to DC current give rise to a magnetizing current pulse with an amplitude much higher for low order harmonics than for high order harmonics. On the other hand, for the single-phase transformer, which represents other core types, the amplitudes of the magnetizing current pulse between low and high order harmonics are more much more uniform.

In Figure 5 it is also observed that the amplitude of the 2nd order harmonic for the single-phase, transformer are, relatively to the amplitude of the 2nd order harmonic for the three-phase transformer, very low. The same goes for other transformers as well, except from the three-phase three-legged core. This is unfortunate because a differential relay set to actuate for low 2nd harmonic components, to distinguish inrush current from fault condition, may lead to erroneous operation during a GIC event.

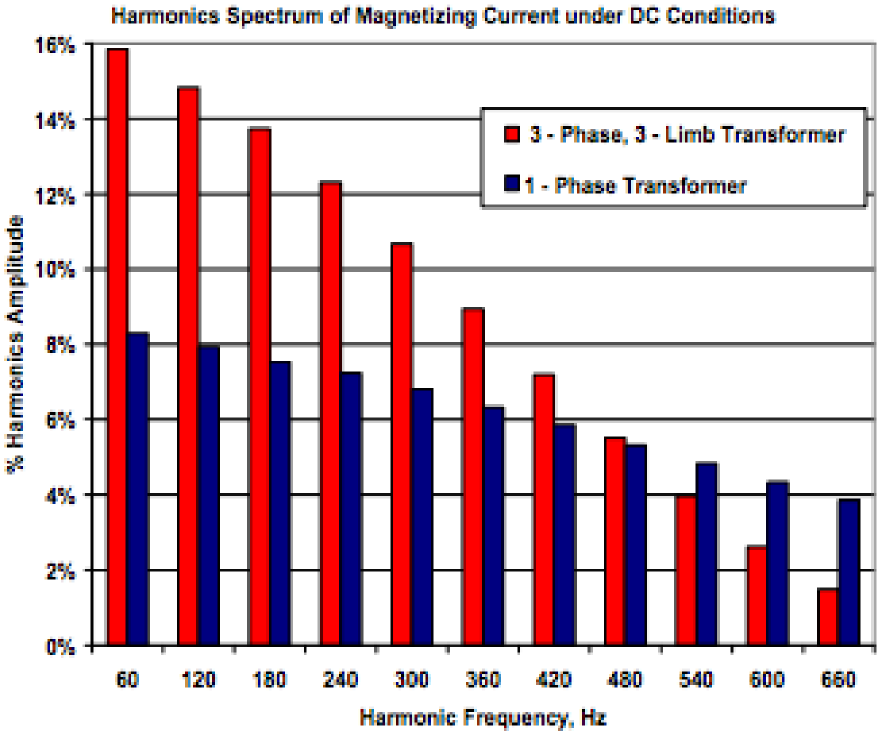

Figure 3.10: Harmonic content of magnetizing current of transformers subjected to DC [Girgis and Vedante].

3.4.2 Reactive Power Consumption

Simulation results from the system configuration in article [Chiesa et al.] confirm that while there is only a minor effect of the GICs on active power, the reactive power consumption of the transformer increases by a factor of 3 when applying 100 A GIC.

In several articles, e.g. [NASA, 2013] and [Chiesa et al.], it is assumed to be a linear relationship between the reactive power consumption of a transformer and the magnitude of GIC. Nevertheless, in the article [Bergsåker, 2014] there was concluded for a type of hybrid transformer that the relationship is non-linear, even though there is an approximately linear region. In the article [Chiesa et al.], on the other hand, using the hybrid transformer model approach [Høidalen et al., 2009], the reactive power consumption as a function of GIC is found to be fully linear.

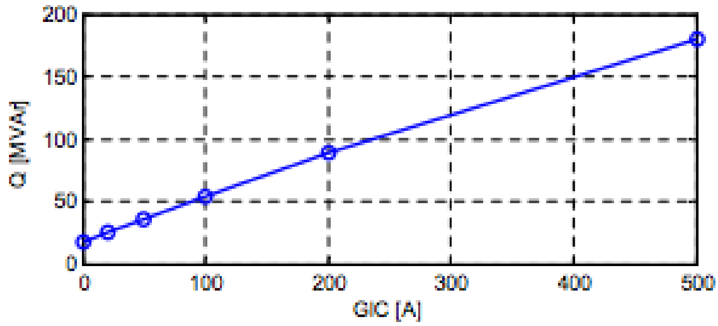

Figure 3.11: Reactive power drawn by a transformer as function of GIC [Chiesa et al.].

The results in the article [Bergsåker, 2014] indicates that an increased cross-sectional area of the transformer leads to a smaller increase in reactive power consumption under the influence of GICs. Accordingly, it is concluded that a larger transformer core will be more resistant to GICs in terms of reactive power consumption [Bergsåker, 2014].

Chapter 4

GIC Simulations using ATPDraw

The simulation program ATP and the plotting program PlotXY can be integrated with ATPDraw [Høidalen]. In this project ATPDraw, Windows version 5.9p3, is the solver used to carry out the simulations.

4.1 GIC modeling

To determine GIC in power lines and earth connections a number of parameters with respect to geomagnetic field, electric field strength and DC voltage induced across the power grid have to be determined. However, for this project the GIC values are predetermined, and only a brief overview of GIC modeling is given.

4.1.1 How to Determine GIC

The occurrence of GIC is dependent on three factors: geometry of the grid, spatial variations of the geomagnetic field, and spatial variations of the ground conductivity [Myllys et al., 2014].

In reality the GICs in the network only depend on one environmental parameter, the geoelectric field. But because of no regular recordings of the geoelectric field close to the power grids one must use numerical modeling to determine the GICs. To achieve this values we must base the simulation on the two geophysical parameters geomagnetic variations and the earth surface impedance [Zheng et al., 2013].

To understand and predict the effects of GICs it is essential to make accurate models of the power grid, its components and their response to GICs. To do so FEM-based models and magnetic circuit models can be used.

The process of modeling GICs in the power system can be divided into three steps: "Calculation of the geoelectric field, DC mapping of the power system, and calculation of GIC flows in the system" [Bernabeu, 2013].

Transformer Model

The transformer models used for GIC study purposes can be devided into two categories: Magnetic models that deal with reactive power consumption and harmonic generation and thermal models that deal with hot spot heating [NERC, 2013]. In this project there are only used magnetic models.

When modeling a transformer one must determine a multitude of parameters. There are three ways to choose these parameters: from factory test reports, from detailed factory design information or, if the basic ratings of the transformer are the only data available, from a complete estimation [Negri and Gotti, 2007].

FEM models

The requirement of detailed design information and the computational burden of the FEM model makes it an unsuitable choice for simulations of the power grid. Nevertheless it is a great option for simulations of the tank and other metallic components where power losses and temperature rises are of concern [Chiesa et al.].

Magnetic Circuit Models

When using models based on magnetic circuit theory to analyze the GIC effects on transformers it is important to take all the necessary parameters into account to get an adequate representation. To do so, topological representation of the core structure with independent core sections and air flux paths needs to be included [Chiesa et al.].

4.1.2 Important Factors

Interdependencies in the power system

In real life there are interdependencies to consider in the power systems, e.g. mitigation of one transformer may lead to higher magnitudes of GIC at a connected transformer nearby, and these should be included in the simulations of GIC effects on the power system. Also, if not modeling the entire power grid, but only a part of it, the rest of the grid should be represented by an equivalent.

In this project only a part of a power grid is modeled. But since it is not part of a specific power system and the circuit diagram given is considered to be sufficient for the purpose of this project, an equivalent replacing the rest of the power system will not be developed.

Air-Core Inductance and Air Path Inductance

It is important to include the air-core inductance to achieve an accurate representation of highly saturated state of the core. Furthermore it is crucial to include off-core flux paths in the model, i.e. include air path inductance, because part of the flux follow paths outside the core, and air paths inductances are shown to be much larger for DC than for 50 Hz [Chiesa et al.]. Not doing so would lead to misleading results, e.g. false values of the harmonic content and the reactive power consumption, which in turn could lead to false tripping of protection relays under the influence of GIC [Chiesa et al.]. Due to the theory in subsection 3.3.4 the deviations will be greater for the three-phase three-legged transformer than for the three-phase five-legged transformer.

In reality the flux forced outside the transformer core has a continuous distribution across space. That is, it could be represented by an infinite number of flux paths on the inside and outside of each winding of the transformer. The transformer models used in this project include off-core flux paths by air path inductance and inductances representing the space between the leg and inner winding, inner winding and middle winding, and middle winding and outer winding.

GIC Signature

In order to conduct realistic simulation studies of the GIC thermal capability of a transformer it would be convenient to use a GIC signature. The GIC signature is based on data from a large number of measured GIC profiles during GMDs and a reference geoelectric profile, and is consisting of a large number of consecutive narrow pulses. These pulses may be divided into two categories, one being low to medium level pulses lasting for a period in the range of hours and the other being high peaks with a duration of a fraction of a minute until several minutes [IEEE, 2015, 7.2.1 Suggested standard GIC signature, p. 25].

Establishing thermal capability of the power transformer is out of scope for this project, and an appropriate GIC signature will not be applied. Nevertheless, it is mentioned because of its utility in the determination of thermal response of a power transformer when establishing power transformer capability.

4.2 Circuit Diagram

The electrical diagram in Figure 4.1, named Model A, was initially intended to use to accomplish the tasks in this project, but it turned out that it was difficult to obtain results without major flaws from this model. So, for the last part of the project, another electrical diagram was used, see Figure 4.2. This test arrangement, called Model B, is based on the article [Lahtinen and Elovaara, 2002].

Model B showed greater accuracy in terms of less noise, less current and voltage spikes, and the findings were more in accordance with the GIC theory. Hence, measurements done in Model B will be assumed to be more relevant. Thus, even though results from using Model A seem to confirm some tendencies seen for Model B, the results from Model A will be left out due to their inaccuracy. Nevertheless, a description of Model A, some measurement methods and a few simple reflections will still be included. The purpose is to discuss errors and deficiencies of model Model A in the discussion part of the report, and in case someone would find interest in carrying out a further investigating of the test arrangement.

Omitting the resistors added to the windings of the transformers in Model A and Model B, whether the winding is isolated from earth or grounded, normally results in error. Therefore, the resistors are needed for the simulation to ensure that the models work properly. This should not be the case and the need for excessive resistances may be due to errors in the source code of ATPDraw.

4.2.1 Model A

The geomagnetic field causing GIC to flow in Model A is represented by a grounded voltage ramp which is connected to the HV side of the 300MVA transformer. The voltage rises from zero to a constant, E0, in one second. To be able to measure the GIC induced by the ramp block a measuring switch is placed between the ramp block and the HV winding.

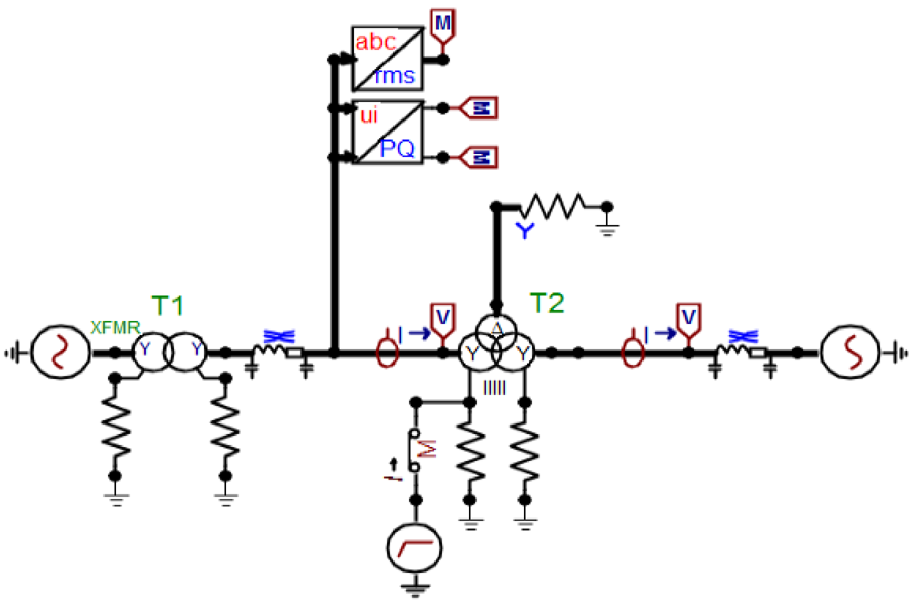

Figure 4.1: Circuit diagram of Model A

4.2.2 Model B

As already stated, the results from Model B is more as expected than for Model A, with respect to the GIC theory. But on the other hand, Model B is not a particularly realistic circuit diagram as the HV side of the two transformers are connected at the same node, i.e. no physical distance. Trying to improve Model B, e.g. adding line impedances, is a laborious work which requires a lot of troubleshooting, and will be left out of the scope of this project due to the time limit.

The GIC is fed into the network from a grounded DC current source which is connected to the HV winding of transformer number two, T2, see Figure 4.2. The DC current source applies a current of a given value and works instantaneously.

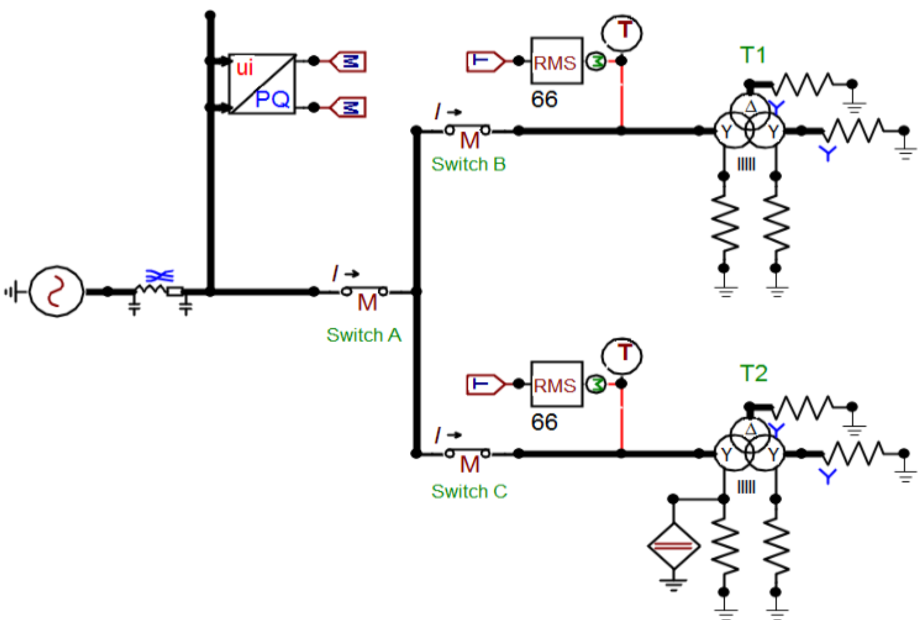

Figure 4.2: Circuit diagram of Model B

Table 4.1: Transformer rating and design for both the 300MVA-5 and the 300MVA-3 transformer model.

HV	420 kV	300 MVA	Y grounded
LV	132 kV	300 MVA	Y grounded
TV	47 kV	100 MVA	Δ

4.3 Transformer model

As the transformer connected to the GIC source there are used two types. The two types mainly have the same ratings and designs, see Table 4.1, except that they have three and five limbs.

4.3.1 300MVA-5

Figure 4.3 shows the electrical diagram of the 300MVA-5 core transformer from ATP-Draw which is working as a passage for GIC to enter the power grid. The transformer is a three-phase, five-legged 300 MVA transformer. Both the high voltage winding on the primary side and the low voltage winding on the secondary side are star connected, and connected to ground by a low resistance path. Furthermore, it has a Δ, isolated from ground by a high resistance path. The Δ can be eliminated from the circuit by opening the switch which can be seen in Figure 4.3.

The upper part of the diagram in Figure 4.3 , except the far right, represents one phase, R, and is repeated three times downwards due to the three phases R, S and T. The total losses in the core are assumed to be divided more or less equally between the eddy current losses and the hysteresis losses, and are represented by RC and LC, respectively. The far right of the circuit represents the yoke with the outer limbs. A list of parameters description is given in Table 4.2.

4.3.2 300MVA-3

The description of the three-phase three-legged transformer, 300MVA-3, is similar to the 300MVA-5 core transformer, see Figure 4.4. The 300MVA-3 core transformer only have three limbs, thus no outer limbs. This taken into account, one can see that the

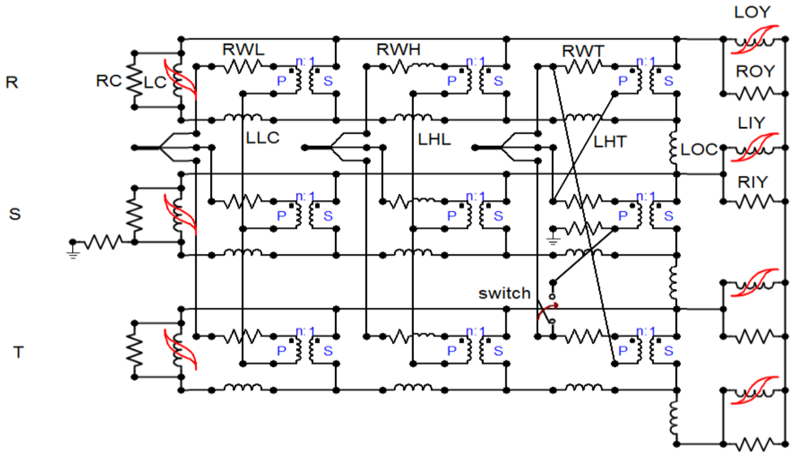

Figure 4.3: Topology of the 300MVA-5 transformer model

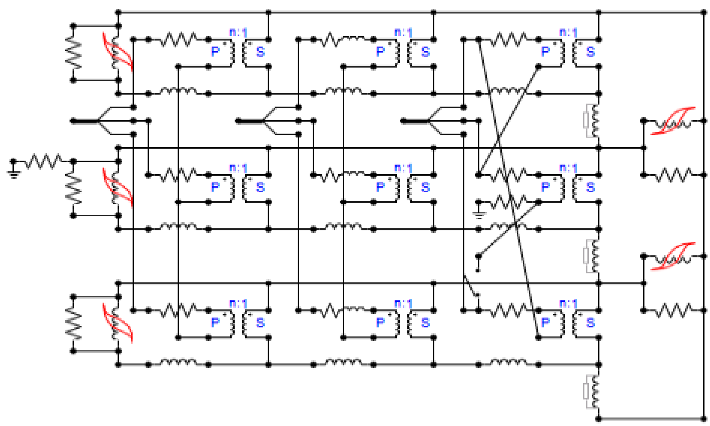

Figure 4.4: Topology of the 300MVA-3 transformer model

topology of the two transformer types are nearly identical, except from to the right in the circuit diagrams, where the 300MVA-3 model is represented by only the yoke, as the limbs are all main legs.

Table 4.2: Parameters description for the 300MVA-5 transformer model, see Figure 4.3. To better get an idea of the parameters description look at the sketch of the "Core Form, 3 phase, 5 limb" in Figure 3.7.

RC	Resistance representing losses in leg
LC	Inductance in leg, may be saturated
RWL	Resistance in LV winding
RWH	Resistance in HV winding
RWT	Resistance in tertiary winding
LLC	Leakage inductance representing the space between the inner winding and the leg
LHL	Leakage inductance between LV winding and HV winding
LHT	Leakage inductance between HV winding and tertiary winding
LOC	Leakage inductance representing the space outside the core, referred to as air path inductance
LOY	Inductance of outer limb, may be saturated
ROY	Resistancerepresenting losses of outer limb
LIY	Inductance of the yoke, may be saturated
RIY	Resistance representing losses of the yoke

4.4 Measurement Methods

In this section the measuring techniques will be described. Most of the methods applies for both Model A and Model B, and it will be specified when this is not the case. For both models the focus will mainly be on the transformer where the GIC enters, T2, and the reactive power flow in the system. This is because the saturation is expected to be the highest in T2.

The main purpose is to investigate how the GIC effects change with respect to certain conditions. Parameters of interest will be, unless otherwise stated, as given in Table 4.3.

Table 4.3: Default values and default settings for Model A and Model B

Parameter	**Default Value/Setting**	**Description**
Tmax	70	End time [s] of simulation.
U_0	420	Generator voltage [kV].
E0	150	The maxiumum voltage [V] induced by the ramp block in Model A.
GIC0	200	The DC current [A] induced by the DC current source in Model B.
TCL	closed (-1)	Closing time [s] of switch in Δ, denoting whether the switch is closed (-1) or open (1000).
LOC	500	Air path inductance [mH] due to each phase.
Power Transformer	300MVA-5	Type of power transformer connected to the GIC source.

The setup of Model B will differ in terms of transformer model, presence of Δ, magnitude of GIC0 and value of LOC. This gives a total of eight different setup configurations, see Figure 4.5. A more detailed explanation will be given in subsections 4.4.1-4.4.4.

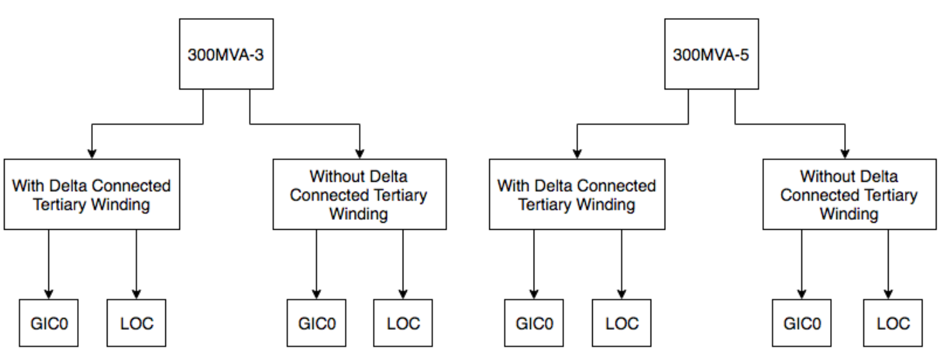

Figure 4.5: The flow chart shows the different combinations that makes up the eight setup configurations used in the project report.

It would be interesting to measure the reactive power consumption, current, voltage and magnetic flux at a large number of nodes to understand the GIC effects on the entire power system and how the different components in the electrical diagram interfers with each other. Nevertheless, the measurements are limited to only a few components. This is for the benefit of comparing several setups, i.e. combinations of 300MVA-3 and 300MVA-5 transformers, with or without a Δ, and for different values of air path inductances and GIC magnitudes.

It is of crucial importance to set the step of simulation, delta T, to adequate values in ATPDraw. In Model A the time step is set to 4 μs. If the time step is reduced by a factor of ten the compilation does not terminate when having an end time of simulation, Tmax, of several tens of seconds. In Model B the time step is set to a value of 40 μs. Increasing the time step in both models by a factor of ten in an attempt to reduce the solving time leads to incorrect results.

The end time of simulation, Tmax, is set to 70 s beacuse the different systems are all found to be in an approximated steady-state at this time.

The effect of GIC on active power loss is in general relatively small, hence, the active power measurements will be disregarded.

4.4.1 Three-Legged and Five-Legged Transformers

The differences between three-phase three-legged and three-phase five-legged transformers when it comes to GIC response will be explored for each of the other tasks. This is simply done by replacing the 300MVA three-winding transformers in a circuit diagram with either all 300MVA-3 or all 300MVA-5 transformer models. This applies to the transformer T2 in Model A, see Figure 4.1, and to both T1 and T2 in Model B, see Figure 4.2.

If using Model A one would measure the current through the connection from the ramp block to the HV winding of the adjacent power transformer. For Model B the GIC magnitude is already given, and the currents of interest are the RMS current and the phase currents across Switch C, see Figure 4.2. When measuring current the factors of interest are the shape, magnitude and harmonics. In addition the reactive power flow in the power system should be measured for both models. Furthermore the flux-linkages in the different sections of the transformer, including off-core flux, should me graphed.

4.4.2 Delta Conntected Tertiary Winding

To find out which impact the Δ has on the GIC effects both the three-legged and the five-legged transformer were tested with and without the Δ.

4.4.3 Air Path Inductance

To find how the effects of GIC change with the air path inductance, i.e. different values of LOC, it is convenient to look at the flux-linkages in different core sections. To do so in ATPDraw one can use the relation

$$|\varepsilon| = \left|\frac{d\phi}{dt}\right| \tag{4.1}$$

and plot the integration of the voltage across the different core sections using the integration function in the PlotXY program. In Equation 4.1 ε is the term for induced voltage [V], ϕ is magnetic flux [Wb] and t is time [s].

The ideal would have been to set the value of LOC to 0 mH, i.e. no flux driven outside the core, and a few higher values to look at the difference in flux-linkages, current in the HV winding of T2 and the reactive power consumption of the system. However, setting LOC to 0 mH or a small value, such as 0,1 mH or 50 mH, is causing trouble when running the simulation in ATPDraw. Therefore, the LOC is set to 250 mH, 500 mH, 750 mH and 1000 mH for the different transformer configurations, assuming that LOC is 0 mH would follow the same pattern pattern. Using the 300MVA-5 without Δ even setting LOC to 250 mH gives an error message when trying to run the simulation, and will be omitted for this particular configuration.

The idea is to visualize the air path inductance influence on the GIC effect. To do so one will compare the magnetic flux through certain parts of the transformer, the air paths included. These are plotted together for different values of the air path inductance, LOC. The paths chosen for the 300MVA-5 transformer, see Figure 4.3 and Figure 4.6, are

LC	Leg
LOY	Outer limb
LIY	Yoke
LOC	Air path

For the 300MVA-3 transformer there are no outer limbs and the magnetic flux is only measured through the leg, yoke and air path, see Figure 4.4 and Figure 4.7,

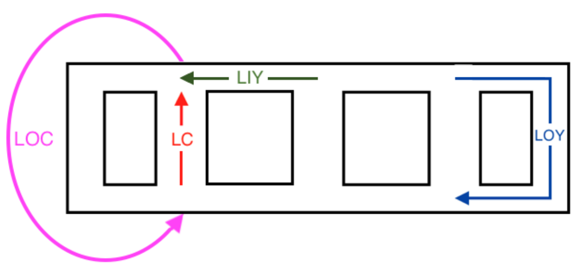

Figure 4.6: The illustration shows a five-legged core transformer model and the flux paths measured in ATPDraw.

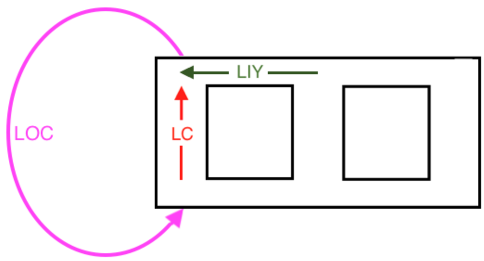

Figure 4.7: The illustration shows a three-legged core transformer model and the flux paths measured in ATPDraw.

4.4.4 Magnitude of the Geomagnetically Induced Electric Field and the size of the GIC

It would be interesting to check how much the GIC effects depend on the magnitude of either the geomagnetically induced electric field or the GIC for Model A and Model B, respectively. For Model A the magnitude of the geomagnetically induced electric field is changed simply by changing the maximum voltage induced by the ramp block. For Model B the magnitude of GIC is changed by choosing different values for the DC current induced by the DC current source. More specific, the value of the DC current source in Model B will be set to 100 A, 200 A and 300 A. To compare with the system when GIC is not induced one replaces the DC current source in an electrical diagram configuration with a small grounded resistance.

4.4.5 X/R ratio

There may exist a relationship between the time constant which describes how fast the GIC is rising, and the X/R ratio of the transformer and its adjacent lines. In the sequence network a transformer is represented as its positive and negative sequence impedances in the positive and negative sequence networks, respectively. The transformer representation in the zero sequence network, however, may have a high complexity [Amberg and Rangel, 2014].

Power lines, and transformers, are passive elements. Given that the three phases of

Table 4.4: Parameters description of the three-phase RLC symmetrical PI-equivalent. The negative sequence impedance components are equal to the components of the positive sequence impedance.

R_0	Resistance in the zero sequence system [Ω/m]
L_0	Inductance in the zero sequence system [mH/m]
C_0	Capacitance in the zero sequence system [μF/m]
R_+	Resistance in the positive sequence system [Ω/m]
L_+	Inductance in the positive sequence system [mH/m]
C_+	Capacitance in the positive sequence system [μF/m]
Length	Length of the line [m]

the line are symmetrical, this implies that the sequence of the applied phase voltages does not matter in regard to the voltage drops across the line. As a result the positive and negative sequence impedances of a symmetrical three-phase transmission line, or a transformer, are assumed to be identical.

The two transmission lines connected to the five-legged transformer in Figure 4.1 are 3-phase RLC symmetrical PI-equivalents. The parameter description for the line is given in Table 4.4.

The total impedance in the line is given by Equation 4.2.

$$Z_{total,line} = Z_+ + Z_- + Z_0 = 2Z_+ + Z_0 = (2R_+ + R_0) + j(2\omega L_+ + \omega L_0 - 2\cdot\frac{1}{\omega C_+} - \frac{1}{\omega C_0}) \quad (4.2)$$

Using Equation 4.2 one can find an X/R ratio for the transmission lines, see Equation 4.3.

$$X/R_{line} = \frac{(2\omega L_+ + \omega L_0 - 2\cdot\frac{1}{\omega C_+} - \frac{1}{\omega C_0}}{2R_+ + R_0} \quad (4.3)$$

Then the X/R ratio for the transformer should be derived and together with the X/R_{line} ratio one could have concluded whether there seems to be a relationship between the GIC time constant and the ratio between the resistance and the reactance in the lines-transformer conjuction.

The idea was to investigate the influence of the X/R-ratio using Model A. But since one ended up using Model B, and this model does not have a realistic line representation, the derivation of the X/R ratio for the transformer as well the simulation testing was omitted from the project. Instead, it will be added as a suggestion for further work.

Chapter 5

Results

In this chapter the most important findings and plots from the simulation testing in ATPDraw, using Model B, will be presented. Furthermore, graphs which are of less importance, or left out for the benefit of good order in the text, will be given in appendices.

Most of the plots for the 300MVA-5 transformer model, as well as some of the plots for the 300MVA-3 transformer model, show big transient values at the beginning of the simulation when when a Δ is not present. Nevertheless, all graphs are adjusted with the purpose of showing how the measured parameters change with time irrespective of the transients.

5.1 Reactive Power Consuption and RMS current of Transformer T2

In Table 5.1 the reactive power consumption and the RMS current flowing into the HV winding of T2 is given for the different configurations of Model B. These are steady-state values, and corresponding graphs are found in Figures B.1-B.16 in Appendix B. For the purpose of visualization the data are also given as column charts in Figures 5.1 and 5.2.

Comparing the different transformers, having the same values of GIC0 and LOC, one see a clear trend. The three-phase five-legged transformer leads to larger steady-state

Table 5.1: The table shows the steady state values for both the reactive power consumption, Q, and the RMS current flowing into the HV winding of T2, I_{T2RMS}, for the different setups of Model B. The column "Delta" states if the transformers do have a Δ or not.

Transformer type	Delta	GIC0 [A]	LOC [mH]	Q [MVAr]	I_{T2RMS} [A]
300MVA-3	With	0	500	0,16	0,22
		100		0,72	33,35
		200		25,95	72,86
		300		59,44	116,52
300MVA-5		0		0,19	0,20
		100		58,19	68,45
		200		113,11	125,63
		300		162,74	177,72
300MVA-3	Without	0		0,16	0,22
		100		0,68	33,34
		200		22,06	69,29
		300		53,58	109,14
300MVA-5		0		0,19	0,19
		100		53,13	52,86
		200		105,82	106,48
		300		155,23	159,50
300MVA-3	With	200	250	2,31	66,77
			500	25,95	72,86
			750	45,15	81,65
			1000	58,60	89,11
300MVA-5			250	107,72	122,66
			500	113,11	125,63
			750	115,70	127,11
			1000	117,26	128,02
300MVA-3	Without		250	1,93	66,71
			500	22,06	69,29
			750	39,50	73,65
			1000	52,70	78,14
300MVA-5			250	-	-
			500	105,82	106,48
			750	108,44	107,92
			1000	110,03	108,91

values for both reactive power consumption in the system, Q, and RMS current flowing into the HV winding of T2, I_{T2RMS}, than for the three-phase three-legged transfomer.

Having a Δ results in higher steady-state values for Q and I_{T2RMS} than without the Δ, with respect to either the 300MVA-3 model or the 300MVA-5 model. However, Figure 5.3 and Figure 5.4 show a much smaller time constant for a transformer without a Δ. That

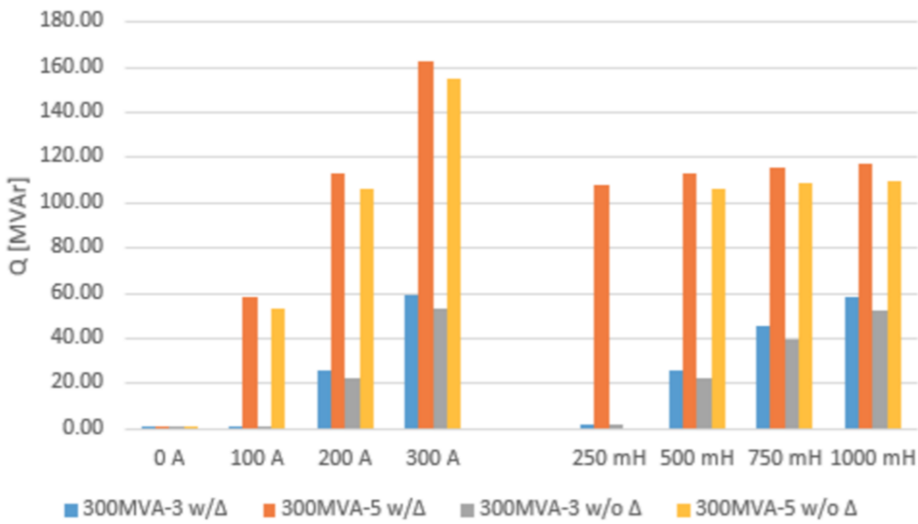

Figure 5.1: The column chart illustrates the reactive power consumption in the system at steady-state for the different setups of Model B. The legends refers to which transformers are used: 300MVA-3 w/Δ, 300MVA-5 w/Δ, 300MVA-3 w/o Δ and 300MVA-5 w/o Δ indicating three-legged with Δ, five-legged with Δ, three-legged without Δ and five-legged without Δ, respectively. The parameters are fixed, as given in Table 4.3, except for either the GIC value, GIC0, or the air path inductance, LOC, which are given on the x-axis.

is, in the beginning Q and I_{T2RMS} are larger for a given transformer without the Δ than for the same transformer having a Δ.

There seem to be a linear relationship between the reactive power consumption and the GIC magnitude for all four transformer configurations used in this project, i.e. both the 300MVA-3 and 300MVA-5 transformer models with and without Δ, see the left side of Figure 5.1. Likewise, it also appears to be a linear relationship between I_{T2RMS} and the GIC magnitude. Furthermore,

Not having a Δ may result in transients with large values for Q and I_{T2RMS} for large values of GIC0 or LOC for both the 300MVA-3 and the 300MVA-5 transformer models, see plots in Appendix B. The maximum values of both Q and I_{T2RMS} may reach values of 5 to 6 times the steady-state values. For the 300MVA-5 transformer model without the Δ there also appears sharp spikes in both Q and I_{T2RMS}, see Figures B.15 and B.16.

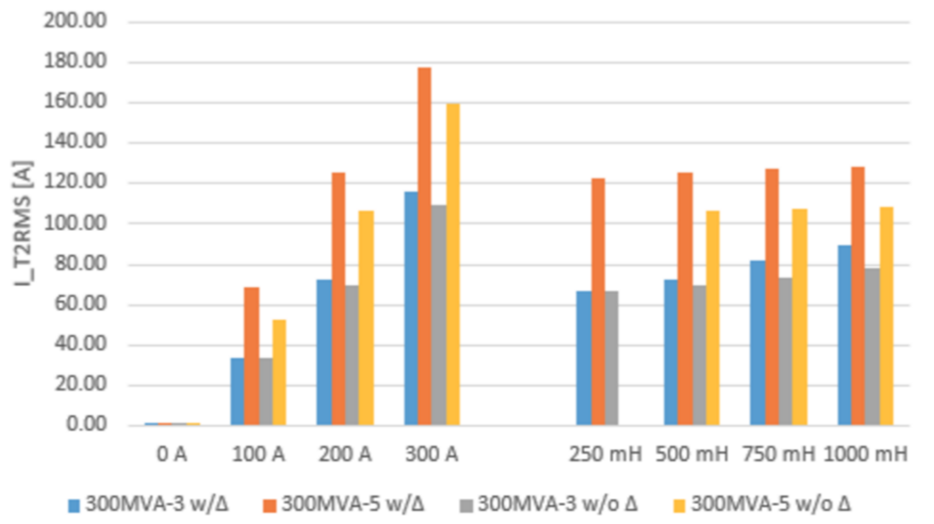

Figure 5.2: The column chart illustrates the RMS currents of transformer T2 at steady-state for the different setups of Model B. The legends refers to which transformers are used: TD, FD, TU and FU stand for three-legged with Δ, five-legged with Δ, three-legged without Δ and five-legged without Δ, respectively. The parameters are set as given in Table 4.3, except for either the GIC value or the air path inductance, LOC, which are given on the x-axis.

5.2 Phase currents of Transformer T2

The graphs in Appendix C show a close-up view of the phase currents flowing into the HV side of the transformer T2 during the test at 200 A DC-current and a LOC value of 500 mH for the different transformer configurations. From the shape one can clearly see that the transformers experience half-cycle saturation. That is, with the exception from for the five-legged transformer without a Δ, see Figure C.4, where the shape of the curves are hard to interpret. Nonetheless, looking more closely at the Figures C.1-C.3 reveals that for the 300MVA-3 transformer model there are a smoother half-cycle saturation shape than for the 300MVA-5 transforme model.

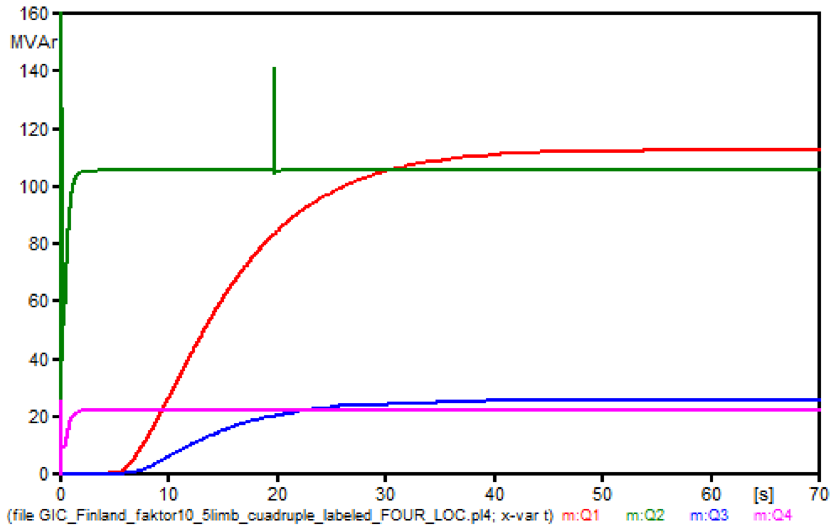

Figure 5.3: Reactive power consumption in the system when GIC0 is 200 A and LOC is 500 mH. The curves represent the tests with the following transformers: 300MVA-5 w/Δ (red), 300MVA-5 w/o Δ (green), 300MVA-3 w/Δ (blue) and 300MVA-3 w/o Δ (pink).

5.3 Harmonic Currents of Phase A of transformer T2

Some plots of the current harmonics of phase A of transformer T2 for the different power transformer configurations are shown in Appendix D, when GIC0 is set to 200 A and LOC is 500 mH.

5.4 Flux-Linkages

When changing the values of LOC the flux in the legs, yoke and limbs did not change significantly. The off-core flux, on the other hand, increases noticeably with the value of LOC. The flux-linkages in different core sections of the transformer T2 for different transformer configurations, when GIC0 is 200 A and LOC is 500 mH, is shown by figures in Appendix E.

The air path flux for the three-phase three-legged transformer with a Δ, see E.1, does not fluctuate. Furthermore, the shape of the air path flux for the 300MVA-5 transformer model without a Δ develops with time, see Figure E.3, while the steady-state shape of

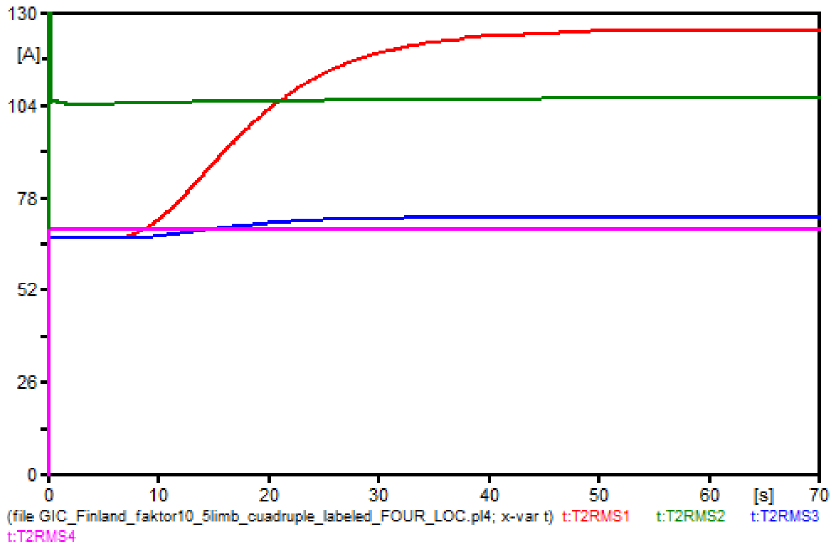

Figure 5.4: RMS current flowing into the HV side of transformer T2 when GIC0 is 200 A and LOC is 500 mH. The curves represent the tests with the following transformers: 300MVA-5 w/Δ Δ (red), 300MVA-5 w/o Δ (green), 300MVA-3 w/Δ (blue) and 300MVA-3 w/o Δ (pink).

the three other transformer configurations appears instantaneously, see Figures E.1, E.7 and E.5. Comparing the air path flux for the different transformer configurations in Appendix E shows that at steady-state there are more flux flowing outside the core for a transformer model with three limbs than with five limbs, see Figure 5.5.

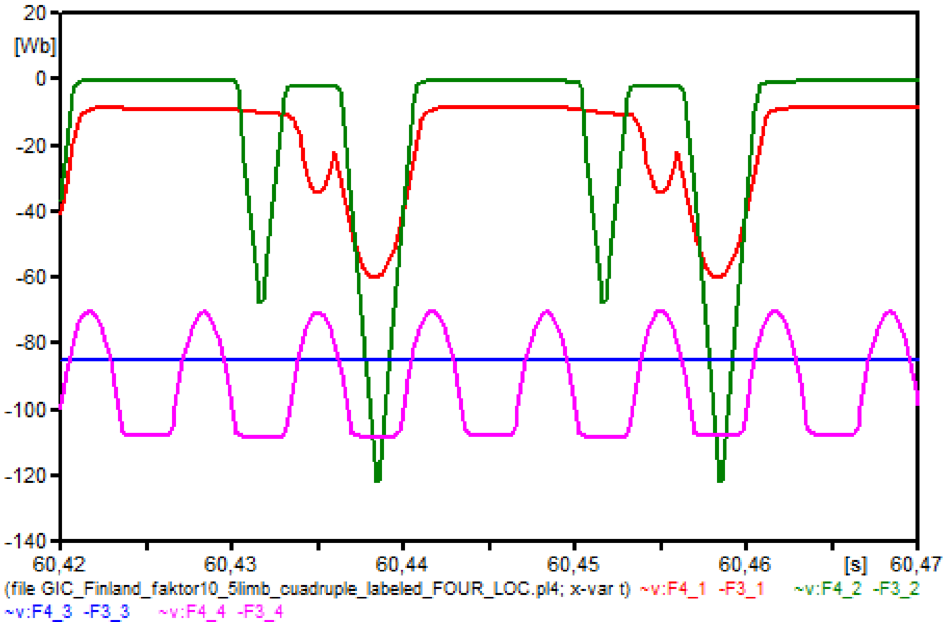

Figure 5.5: The figure shows the the air path flux for the different transformer configurations when GIC0 is 200 A and LOC is 500 mH. The curves represent the 300MVA-5 w/Δ (red), the 300MVA-5 w/o Δ (green), the 300MVA-3 w/Δ (blue) and the 300MVA-3 w/o Δ (pink).

Chapter 6

Summary and Recommendations for Further Work

Recommend further work: Thermal model.

6.1 Summary and Conclusions

The overriding purpose of this Master's project was to better understand GIC effects on power transformers. To accomplish that goal it became necessary to reach some prerequisite goals. Chapters 2 and 3 concerns solar storms, GICs and their effects on power systems and power transformers. It is presented in the form of theoretical knowledge, referring to related work, and an introduction to the most important historical events is given.

In chapter 4 the circuit diagram, as well as the power transformer models, used in this project are presented. In addition, a few comments on how to determine the GIC magnitude are included. Simulations are performed using ATPDraw, and the results are graphed using the plotting program PlotXY. As mentioned, initially a circuit diagram model with a geomagnetically induced current applied was used for the simulations, see subsection 4.2.1. But since it was difficult to obtain results without major flaws from this circuit diagram it was replaced by another one with a DC current source representing the GIC instead of a voltage ramp block, see subsection 4.2.2. Furthermore, the measurement methods used in the investigation of how the GIC effects are influenced by the conditions given in the main objectives are explained. Due to the change of circuit diagram to a model which is less realistic with respect to power lines the investigation of the X/R ratio was omitted.

The simulations are done using the different transformer configurations, i.e. three-phase three-legged transformer or three-phase five-legged transformer with or without Δ. The parameters which have been modified are the value of the air path inductance and the magnitude of the DC-current applied to the HV winding of transformer T2. The results of the simulations are given in chapter 5 and Appendices B-E. Current harmonics plots of the phase current A of the different transformer configurations are to be found in Appendix D. A discussion based on harmonics will not be given due to shortage of time.

6.2 ATPDraw

Major challenges with respect to the simulations in ATPDraw were experienced during the project work. This fact led to that a greater proportion of the time than planned was spent developing a functional circuit diagram. Thus, when such a diagram was aquired, there was not much time left before the deadline of the Master's project, which imposed limitations on the thoroughness and extention of the work. Some of the challenges were

- running the simulation several times for the exact same circuit model sometimes gave different results,
- in some very few cases a circuit diagram in ATPDraw which worked fine stopped working after saving the ACP file,
- normally adding big or small grounded resistances between the transformer windings and ground were necessary to be able to run the simulations, but in a few apparently inexplicable cases they had to be removed for the model to work properly,

- small values of LOC normally resulted in error when running the simulation,
- ATPDraw frequently froze or stopped working when running simulations or plotting the results, loosing all the results and having to reinitiate the program,
- and one was not able to make the circuit diagram Model A work properly.

Reasons for why Model A, see subsection 4.2.1, did not provide usable results may be numerous. It might be due to

- errors in the source code of ATPDraw,
- issues related to the use of a voltage source to represent the GIC,
- the possibility of the GIC being harder to distinguish from other effects for Model A than for Model B,
- or it might be that Model A is more sensitive to the value of the time step.

Decreasing the time step value from 4 μs to 0,4 μs drastically increases the quality of the results for Model A, but the plots still includes spikes and irregularities which are difficult to explain. A further reduction of the time step value results in error, but enabeling such a reduction would probably increase the quality of the results even more. For Model B there often were difficulties with running the simulation when choosing time step values smaller than 20 μs. Thus, in the end, a time step value of 40 μs was chosen for Model B. Considering the high frequencies present in electrical power systems, 40 μs is a relatively large time step value and may compromise the results.

6.3 Discussion

The main focus during this project have been on the simulations in ATPDraw and the GIC effects on power transformers. And thus, that is what will be discussed in this part.

The simulation results are only digital. In other words they are not verified by values of real life recordings. Consequently, the veracity of the results are questionable. Nevertheless, a major part of the results are in accordance with the GIC theory, e.i. linear relationship between Q and GIC magnitude and three-legged transformers being less suceptible to GIC than five-legged transformers. Therefore, although values may not excact, it is likely to assume that most of the results are fairly reasonable with respect to trends. An exception is the simulations done using the 300MVA-5 w/o Δ, which in general gave unexpected plots. It gave large current spikes and big transient values Figure B.16, not the typical half-cycle saturation pattern for the phase currents, see Figure C.4, and were not able to run even for a LOC value as high as 250 mH. All the peculiarities just mentioned give reasons to doubt all the results coming from the tests using the 300MVA-5 w/o Δ. Nonetheless, the fact that the steady-state values follows the increasing pattern for Q and I_{T2RMS} when increasing GIC0 and LOC, see Figures 5.1 and 5.2 show some credibility.

As expected, five-legged transformers showed greater susceptibility to GIC than three-legged transformers. Furthermore, having a Δ resulted in smaller steady-state values of Q and I_{T2RMS}, even though the time step was smaller such that for a period of time the values where higher than for the same transformer with

The the smoother curves of the air-path flux of three-legged transformers may be due to the fact that there are no return flux paths through the core. In other words, the three-legged transformer will experience half-cycle saturation a for a larger portion of time than five-legged transformers under the same conditions. That is may also be seen by the large flux values of the air path flux for three-legged transformers, 100 Wb, while for the five-legged transformer it fluctuates around 0 Wb.

Finally, with respect to GIC effects, one may draw the conclusion that one should choose three-phase three-legged transformers over three-phase five-legged transformers without a Δ due to its resistance against GIC. Also, it would be interesting to look into the possibility of closing the Δ at the point were the reactive power consumption of the three-legged transformer with and without a Δ

6.4 Recommendations for Further Work

The research that has been undertaken for this project has highlighted a number of topics on which further research would be beneficial. Possible extensions to this Master's project could be as given:

- Develop Model A in terms of adding power lines, loads, transformers and entrances and exit points. Then, one could study the secondary effects, i.e. GIC effects on the other components in the power grid. It would also be possible to continue with the X/L ratio testing, see subsection 4.4.5. In addition one should advance with the interpretation of current harmonics.

- Research whether there is a way to use the Δ in a transformer to mitigate the GIC effects. One way to do this would be to see how the measurements, e.i. reactive power consumption, would react when the switch in the Δ closes at the point of where the reactive power consumption is equal for a transformer with or without Δ during GMDs, see Figure 5.3.

- Develop a functional circuit diagram in ATPDraw which uses a current source to induce GIC.

- Develop a circuit diagram model in ATPDraw with temperature dependent impedances which take into account the heating of the transformer parts. The first step would be to perform real life GIC testing to find the correlations between heating of the different parts of the transformer and phase currents of the transformer. Then, this information could be used to program GIC dependent impedance moduls which acts as temperature dependent.

- The simulations done in this project are rather short compared to the duration of potential large GMDs. Thus, it would be interesting to know how the transformer, e.i. transformer T2 in Model A, would be affected during a more realistic GIC scenario, see the part about GIC signatures in subsection 4.1.2.

- Adjust Model A so that the results fits real life recordings. An example of this has already been done by the supervisor for this Master's project. He obtained a remarkable fit for the reactive power consumption of the five-legged transformer in ATPDraw and recorded apparent power in [Lahtinen and Elovaara, 2002].

Appendix A

Acronyms and Notations

AC Alternating Current

Δ Delta connected tertiary winding

EMF Electromotive Force

EMTP Electromagnetic Transients Program

GIC Geomagnetic Induced Current

GIC0 Magnitude of the DC current [A], representing the GIC, flowing into the ground connection of transformer T2

GMD Geomagnetic Disturbances

GMS Geomagnetic Storm

HV High Voltage

IEEE Institute of Electrical and Electronics Engineers

$\mathbf{I_{T2RMS}}$ The current [A] flowing into the HV side of the transformer T2

LOC Value of the air path inductance [mH] input to the 300MVA transformer model representing the off-core flux paths

LV Low Voltage

MVA Mega-Volt Ampere

NTNU Norwegian University of Science and Technology

Q The reactive power consumption [VAr] in the system

RMS Root Means Square

300MVA-5 w/o Δ Three-phase five-legged transformer model without a delta connected tertiary winding

300MVA-5 w/Δ Three-phase five-legged transformer model with a delta connected tertiary winding

300MVA-3 w/o Δ Three-phase three-legged transformer model without a delta connected tertiary winding

300MVA-3 w/Δ Three-phase three-legged transformer model with a delta connected tertiary winding

T1 Transformer number one

T2 Transformer number two

Appendix B

Combination graphs, Q, T2RMS

B.1 Introduction

The graphs shows the reactive power consumption and the RMS currents of transformer T2 for the different setups of Model B shown in Figure 4.5.

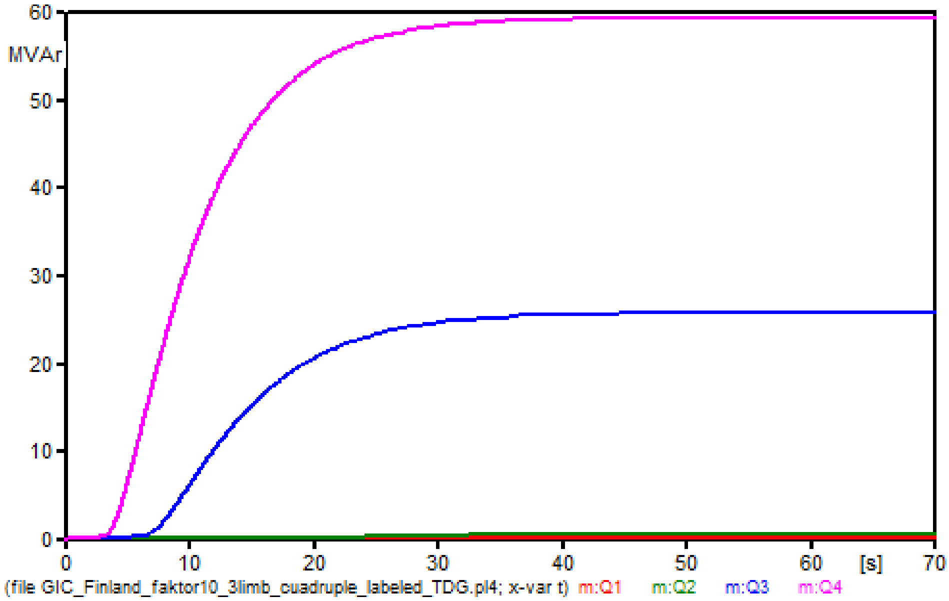

Figure B.1: Reactive power consumption due to a 300MVA-3 w/Δ when changing the GIC value and LOC is 500 mH. The curves represent the tests of the following DC-currents: 0 A (red), 100 A (green), 200 A (blue) and 300 A (pink).

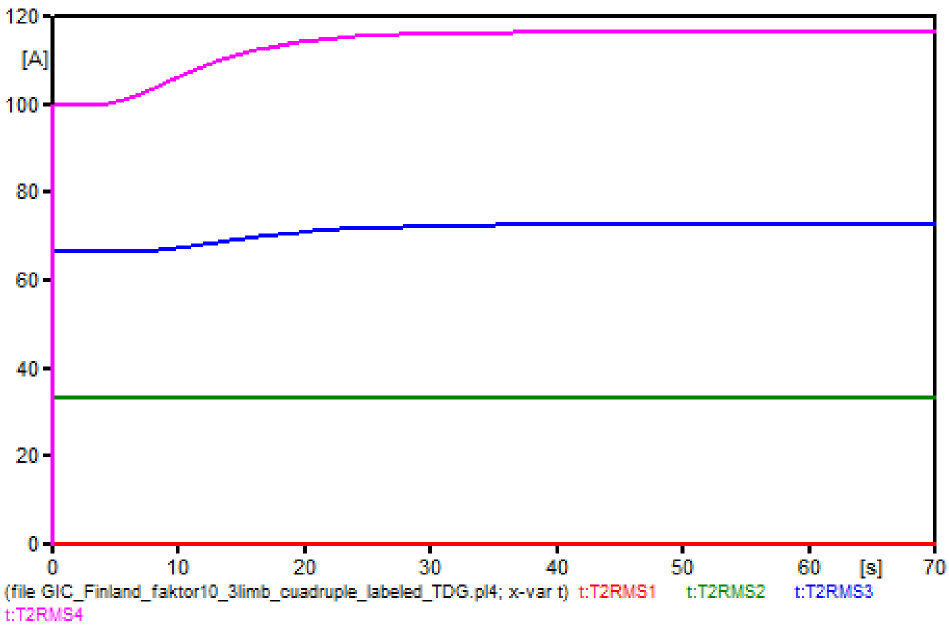

Figure B.2: RMS current flowing into the HV side of transformer T2 when using a 300MVA-3 w/Δ. The GIC value is changed, while the LOC is 500 mH. The curves represent the tests of the following DC-currents: 0 A (red), 100 A (green), 200 A (blue) and 300 A (pink).

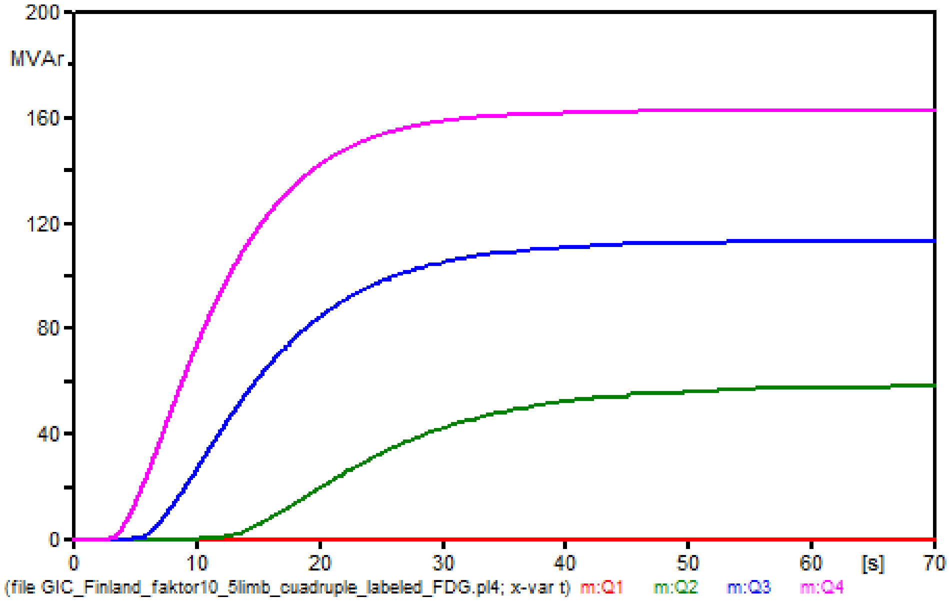

Figure B.3: Reactive power consumption due to a 300MVA-5 w/Δ when changing the GIC value and LOC is 500 mH. The curves represent the tests of the following DC-currents: 0 A (red), 100 A (green), 200 A (blue) and 300 A (pink).

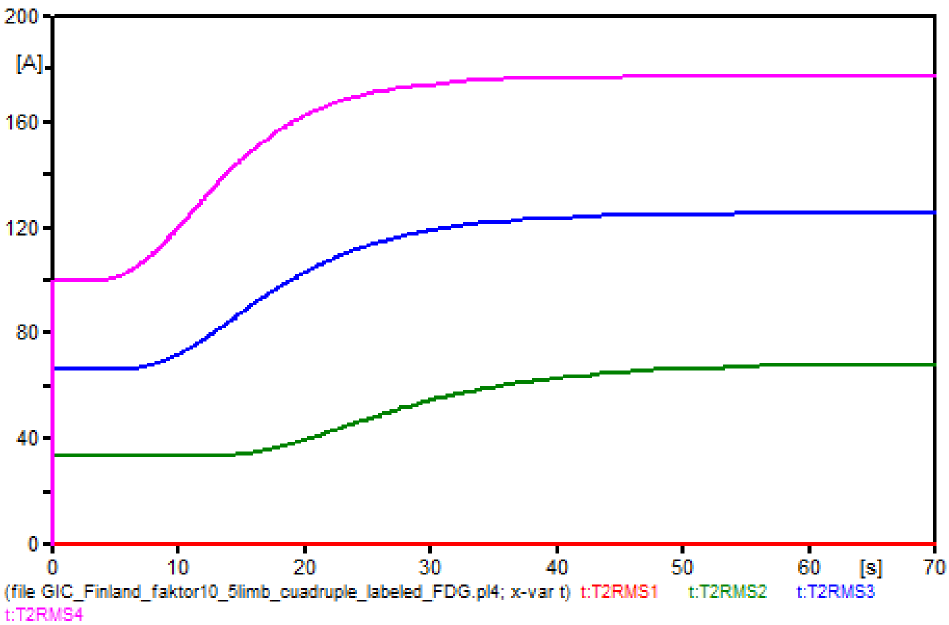

Figure B.4: RMS current flowing into the HV side of transformer T2 when using a 300MVA-5 w/Δ. The GIC value is changed, while the LOC is 500 mH. The curves represent the tests of the following DC-currents: 0 A (red), 100 A (green), 200 A (blue) and 300 A (pink).

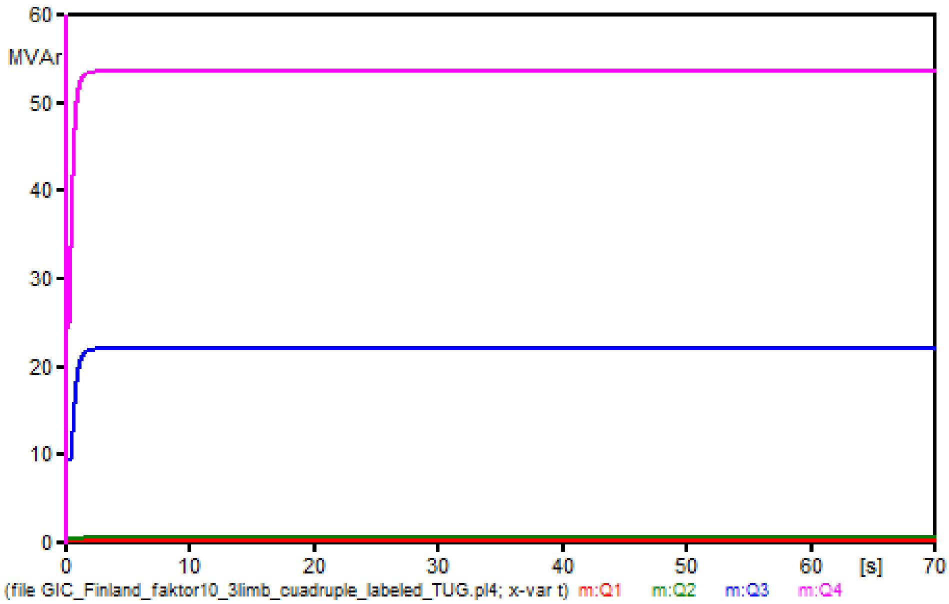

Figure B.5: Reactive power consumption due to a 300MVA-3 w/o Δ when changing the GIC value and LOC is 500 mH. The curves represent the tests of the following DC-currents: 0 A (red), 100 A (green), 200 A (blue) and 300 A (pink).

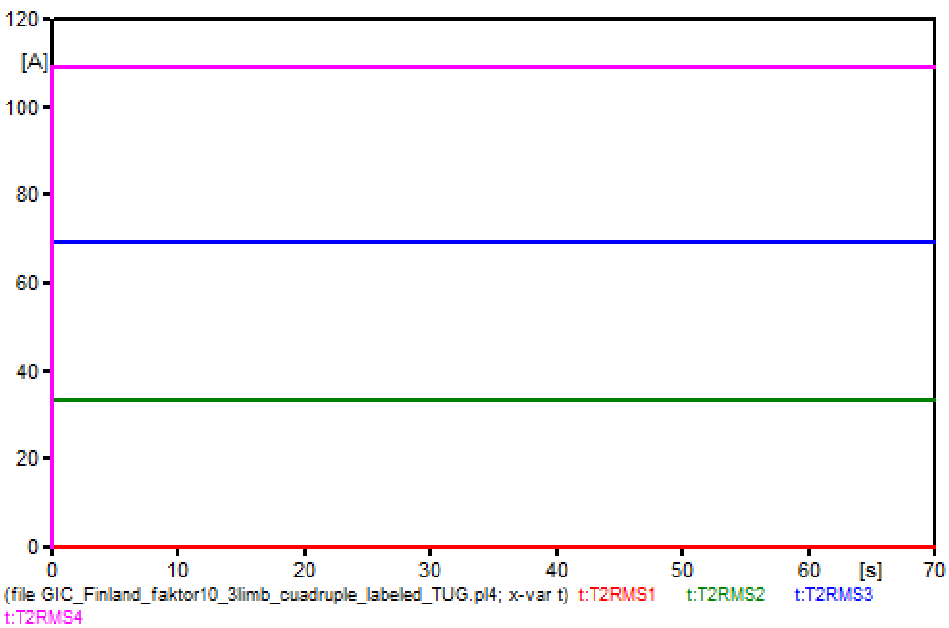

Figure B.6: RMS current flowing into the HV side of transformer T2 when using a 300MVA-3 w/o Δ. The GIC value is changed, while the LOC is 500 mH. The curves represent the tests of the following DC-currents: 0 A (red), 100 A (green), 200 A (blue) and 300 A (pink).

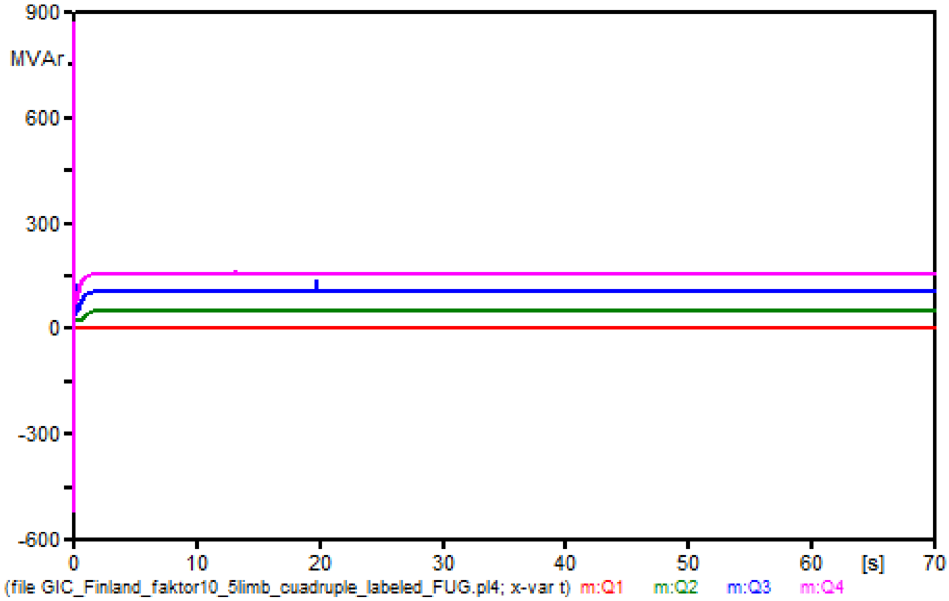

Figure B.7: Reactive power consumption due to a 300MVA-5 w/o Δ when changing the GIC value and LOC is 500 mH. The curves represent the tests of the following DC-currents: 0 A (red), 100 A (green), 200 A (blue) and 300 A (pink).

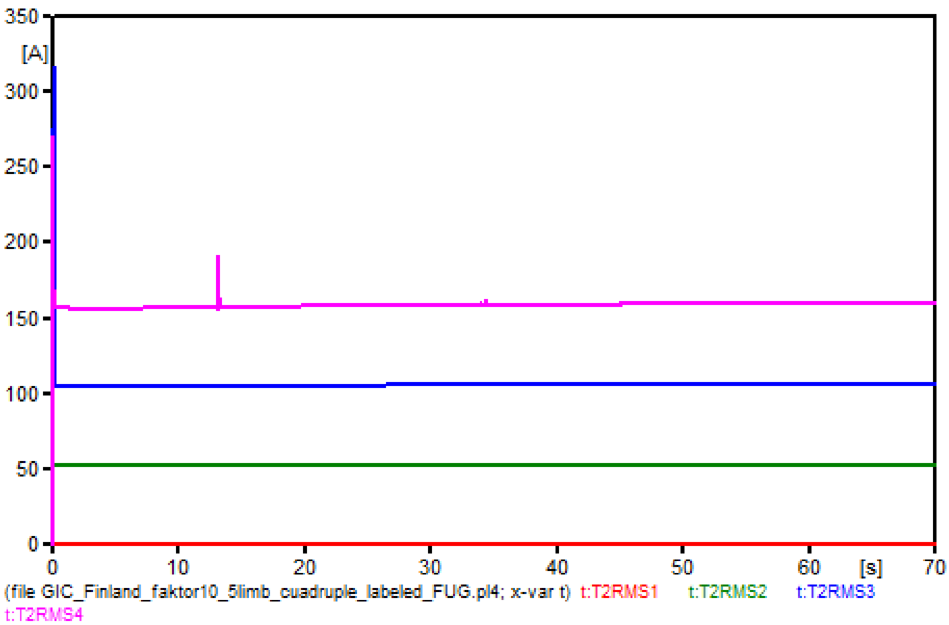

Figure B.8: RMS current flowing into the HV side of transformer T2 when using a 300MVA-5 w/o Δ. The GIC value is changed, while the LOC is 500 mH. The curves represent the tests of the following DC-currents: 0 A (red), 100 A (green), 200 A (blue) and 300 A (pink).

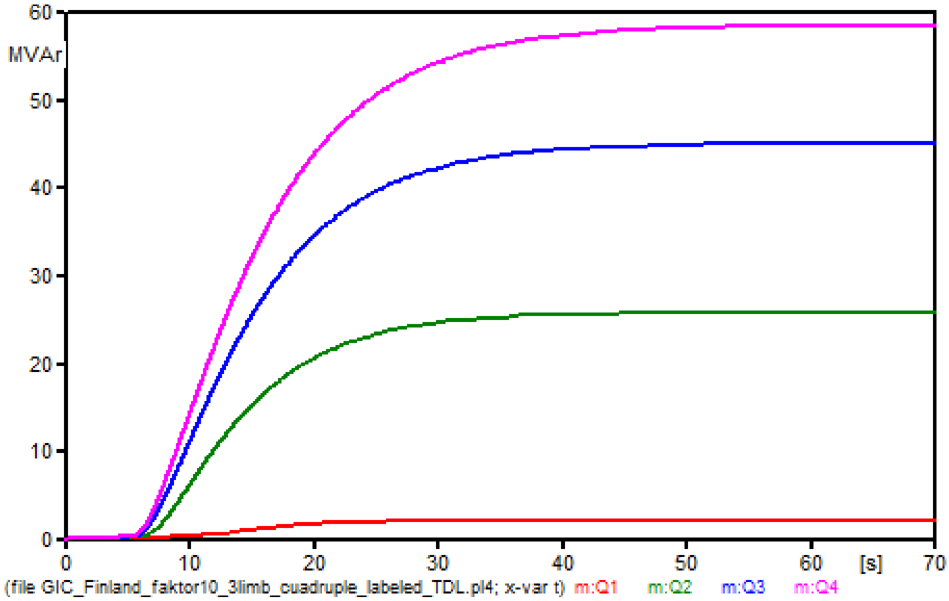

Figure B.9: Reactive power consumption due to a 300MVA-3 w/Δ when changing the LOC value and GIC0 is 200 A. The curves represent the tests of when LOC is set to a value of 250 mH (red), 500 mH (green), 750 mH (blue) and 1000 mH (pink).

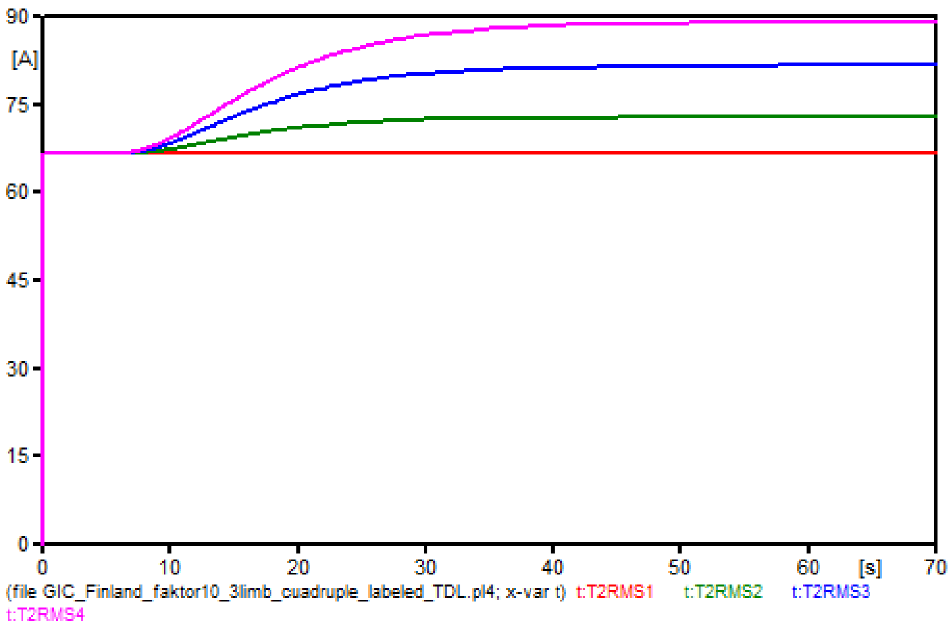

Figure B.10: RMS current flowing into the HV side of transformer T2 when using a 300MVA-3 w/Δ. The LOC value is changed, while the GIC0 is 200 A. The curves represent the tests of when LOC is set to a value of 250 mH (red), 500 mH (green), 750 mH (blue) and 1000 mH (pink).

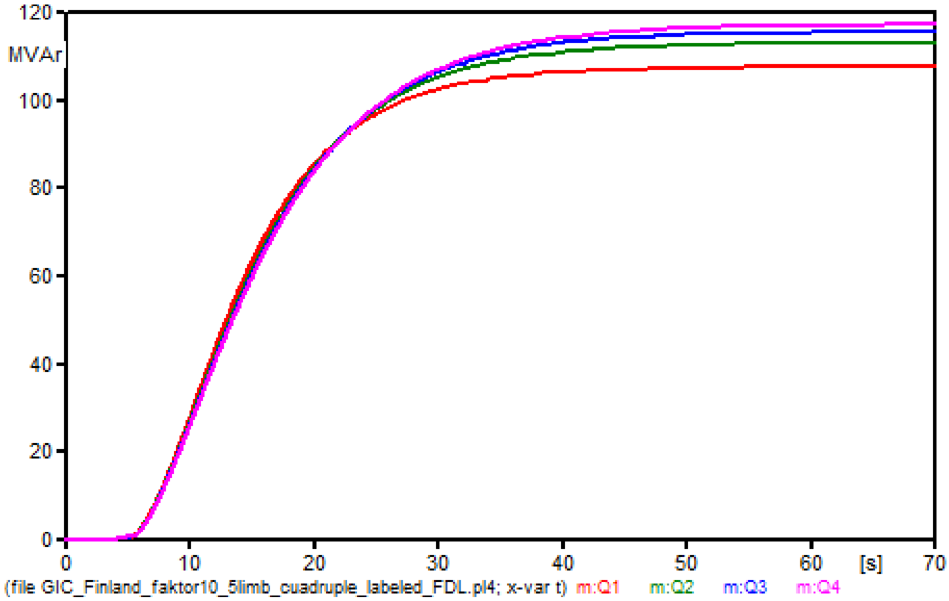

Figure B.11: Reactive power consumption due to a 300MVA-5 w/Δ when changing the LOC value and GIC0 is 200 A. The curves represent the tests of when LOC is set to a value of 250 mH (red), 500 mH (green), 750 mH (blue) and 1000 mH (pink).

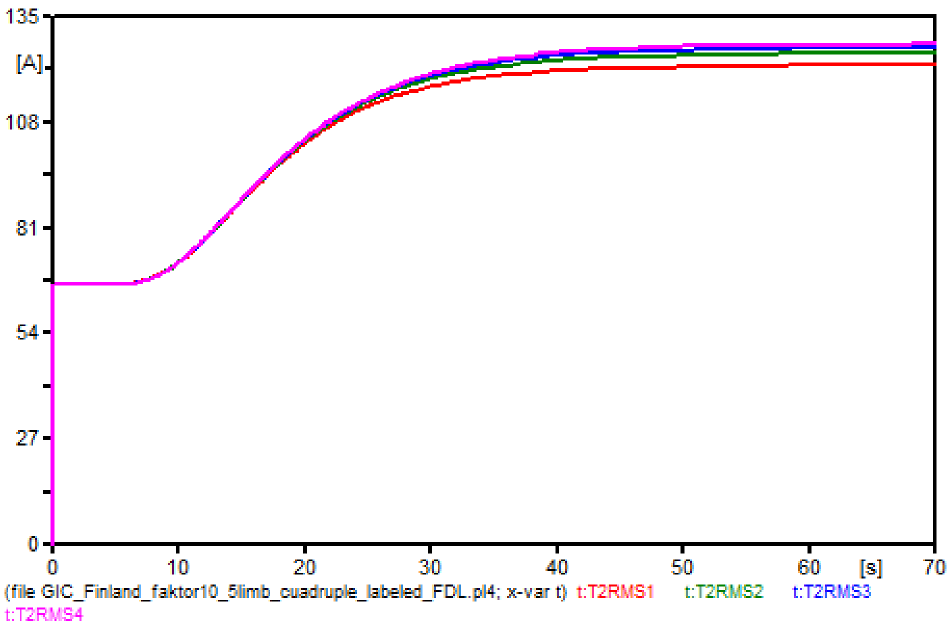

Figure B.12: RMS current flowing into the HV side of transformer T2 when using a 300MVA-5 w/Δ. The LOC value is changed, while the GIC0 is 200 A. The curves represent the tests of when LOC is set to a value of 250 mH (red), 500 mH (green), 750 mH (blue) and 1000 mH (pink).

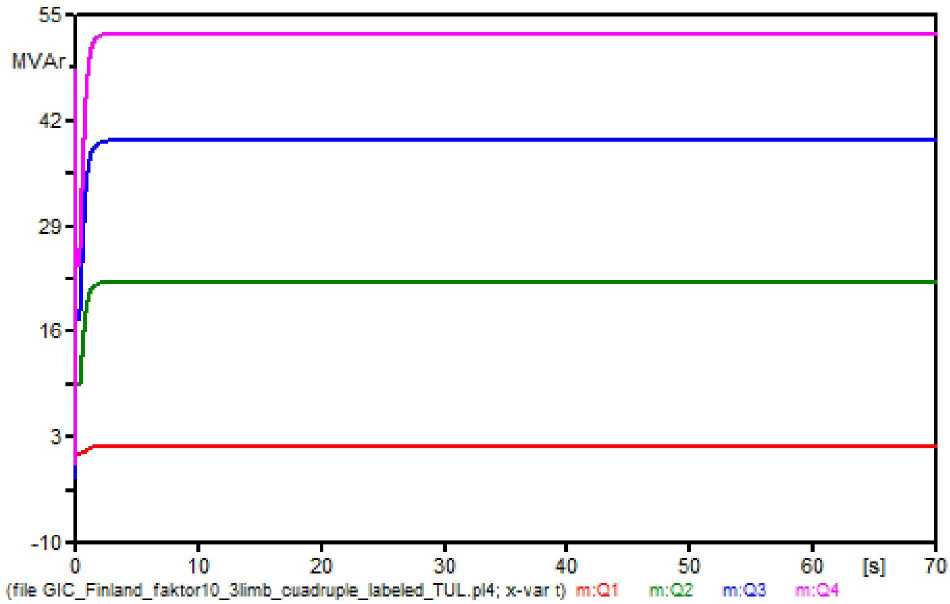

Figure B.13: Reactive power consumption due to a 300MVA-3 w/o Δ when changing the LOC value and GIC0 is 200 A. The curves represent the tests of when LOC is set to a value of 250 mH (red), 500 mH (green), 750 mH (blue) and 1000 mH (pink).

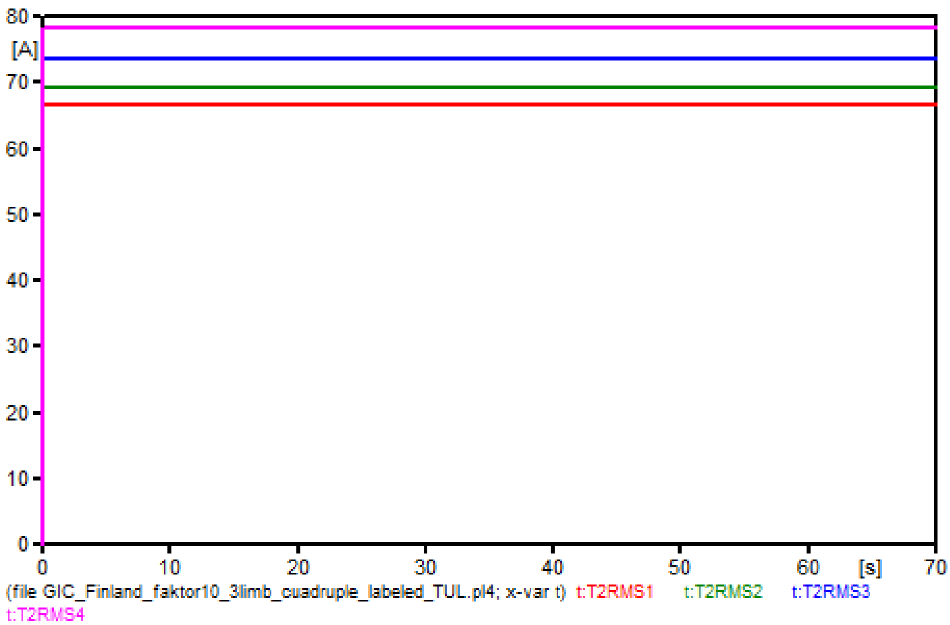

Figure B.14: RMS current flowing into the HV side of transformer T2 when using a 300MVA-3 w/o Δ. The LOC value is changed, while the GIC0 is 200 A. The curves represent the tests of when LOC is set to a value of 250 mH (red), 500 mH (green), 750 mH (blue) and 1000 mH (pink).

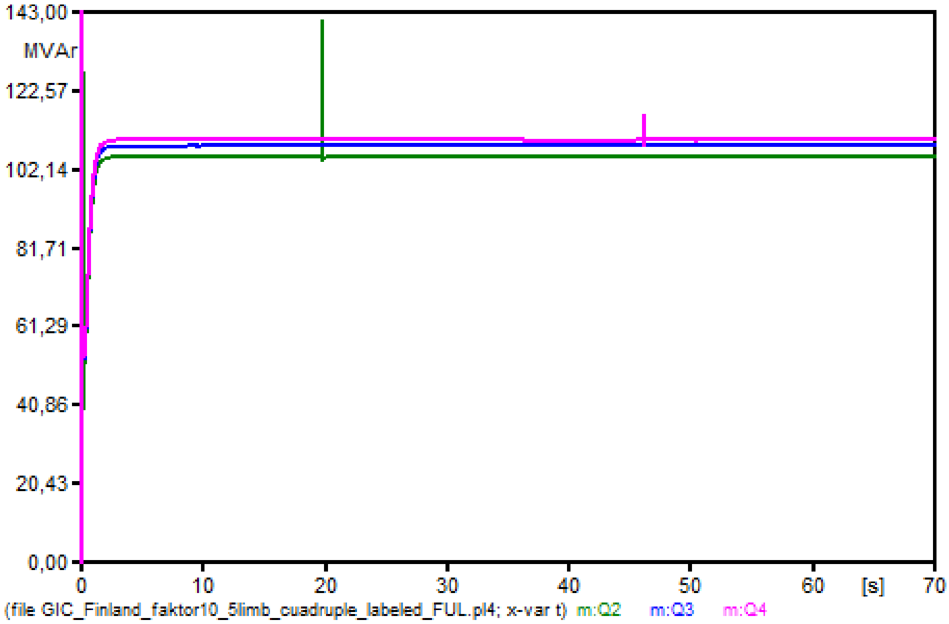

Figure B.15: Reactive power consumption due to a 300MVA-5 w/o Δ when changing the LOC value and GIC0 is 200 A. The curves represent the tests of when LOC is set to a value of 500 mH (green), 750 mH (blue) and 1000 mH (pink).

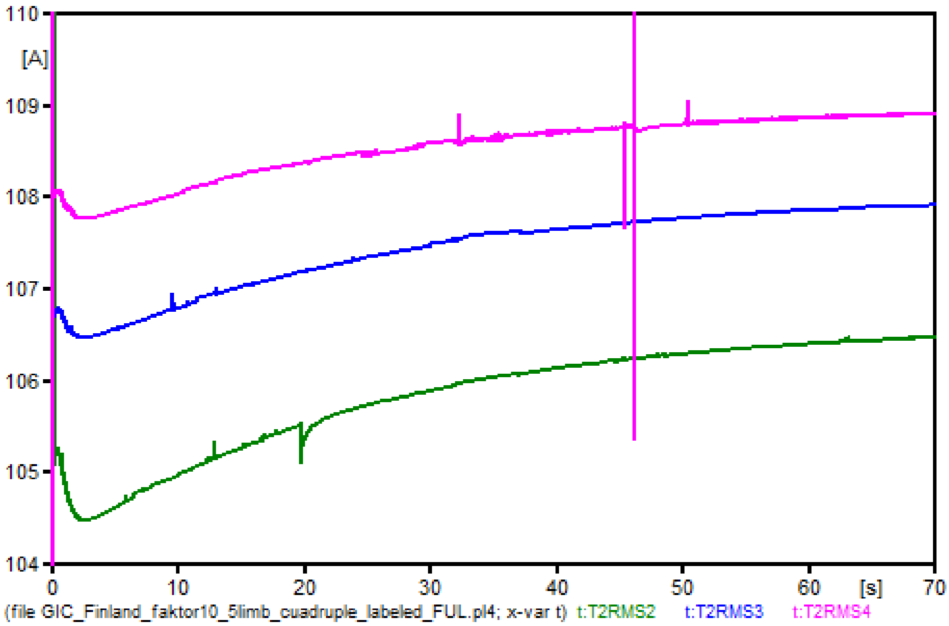

Figure B.16: RMS current flowing into the HV side of transformer T2 when using a 300MVA-5 w/o Δ. The LOC value is changed, while the GIC0 is 200 A. The curves represent the tests of when LOC is set to a value of 500 mH (green), 750 mH (blue) and 1000 mH (pink).

Appendix C

Phase Currents

C.1 Introduction

The graphs shows the three phase currents flowing into the HV winding of transformer T2 for the different transformer configurations in Model B when the GIC, GIC0, is 200 A and the air path inductance, LOC, is 500 mH.

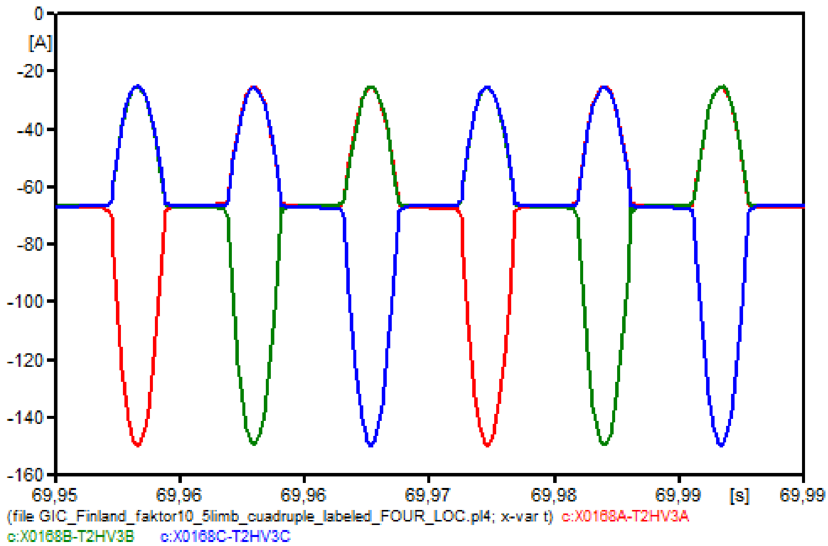

Figure C.1: Phase currents of phases A (red), B (green) and C (blue) flowing into the HV side of transformer T2 during the test at 200 A DC-current and LOC is 500 mH when using a 300MVA-3 w/Δ.

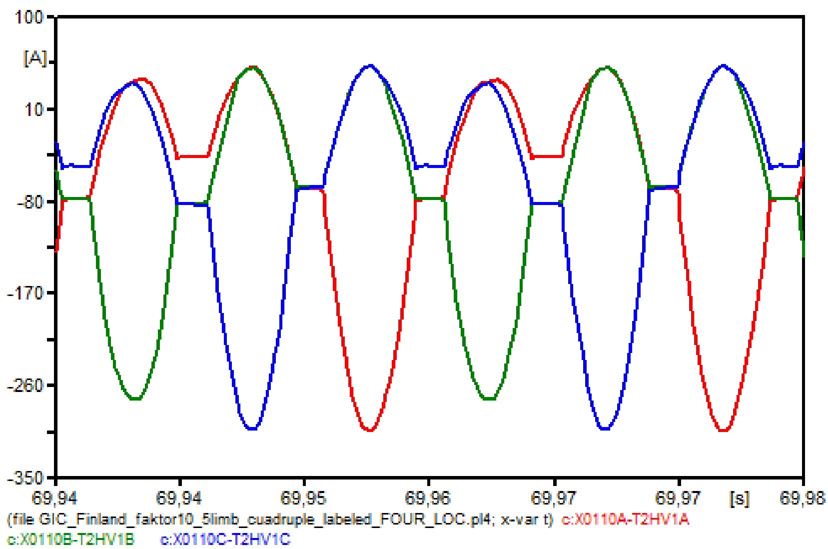

Figure C.2: Phase currents of phases A (red), B (green) and C (blue) flowing into the HV side of transformer T2 during the test at 200 A DC-current and LOC is 500 mH when using a 300MVA-5 w/Δ.

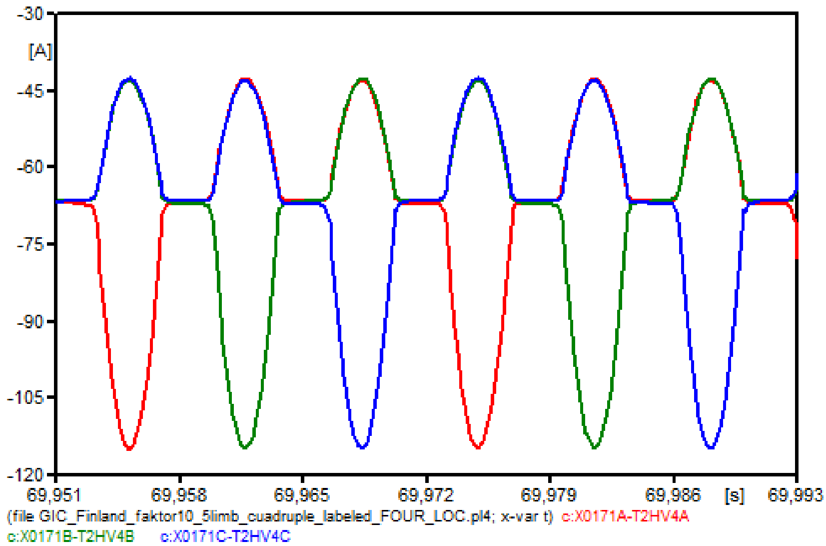

Figure C.3: Phase currents of phases A (red), B (green) and C (blue) flowing into the HV side of transformer T2 during the test at 200 A DC-current and LOC is 500 mH when using a 300MVA-3 w/o Δ.

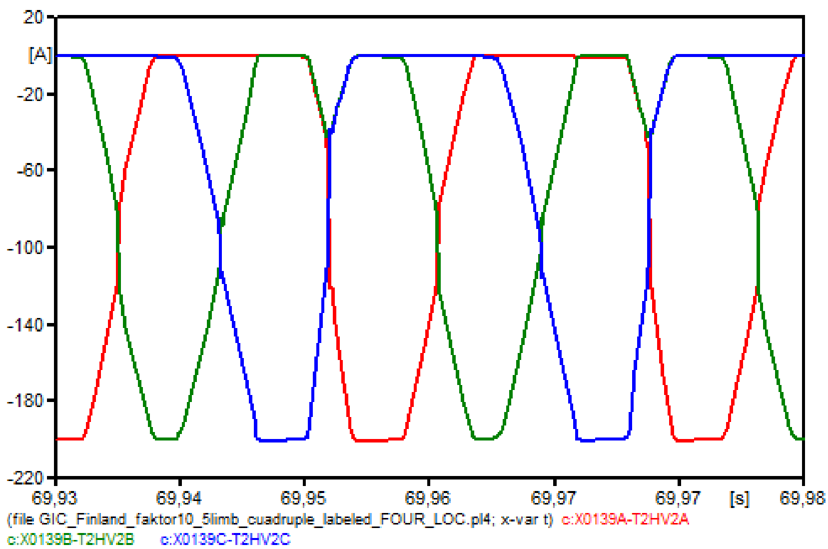

Figure C.4: Phase currents of phases A (red), B (green) and C (blue) flowing into the HV side of transformer T2 during the test at 200 A DC-current and LOC is 500 mH when using a 300MVA-5 w/o Δ.

Appendix D

Current Harmonics

D.1 Introduction

This appendix shows the current harmonics of phase A of transformer T2 for the different power transformer configurations. GIC0 is set to 200 A and LOC is 500 mH.

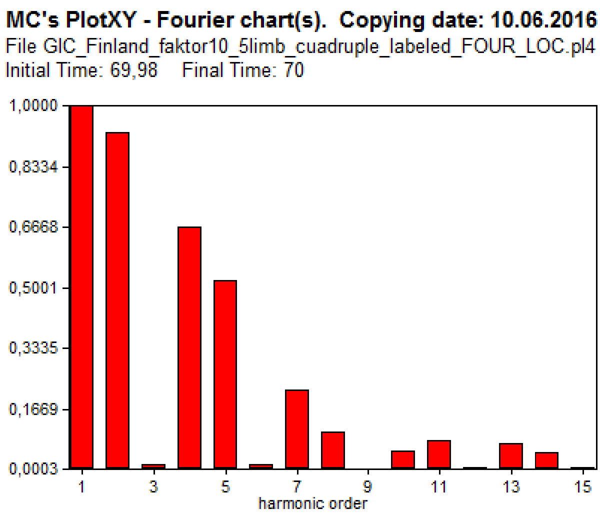

Figure D.1: Current harmonics of phase A of a 300MVA-3 wΔ, when GIC0 is 200A and LOC is 500 mH.

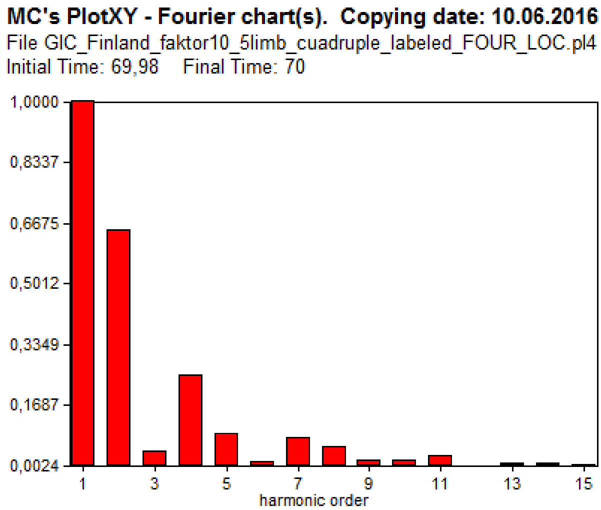

Figure D.2: Current harmonics of phase A of a 300MVA-5 wΔ, when GIC0 is 200A and LOC is 500 mH.

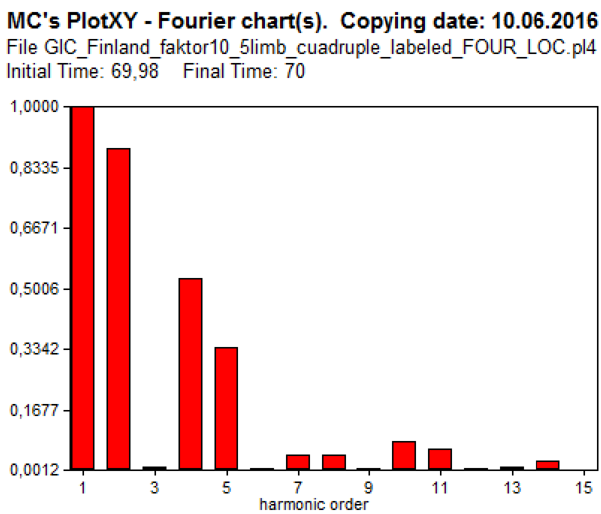

Figure D.3: Current harmonics of phase A of a 300MVA-3 w/o Δ, when GIC0 is 200A and LOC is 500 mH.

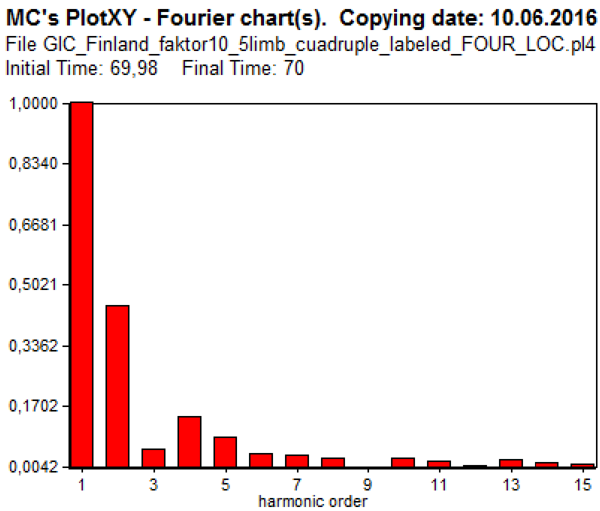

Figure D.4: Current harmonics of phase A of a 300MVA-5 w/o Δ, when GIC0 is 200A and LOC is 500 mH.

Appendix E

Flux Distribution

E.1 Introduction

The graphs shows the flux-linkages in different core sections of transformer T2 for the different transformer configurations in Model B. The GIC, GIC0, is 200 A and the air path inductance, LOC, is 500 mH. There are two graphs for every transformer configuration, the first showing the results for the first 70 seconds and the second showing a section of about two cycles at steady-state.

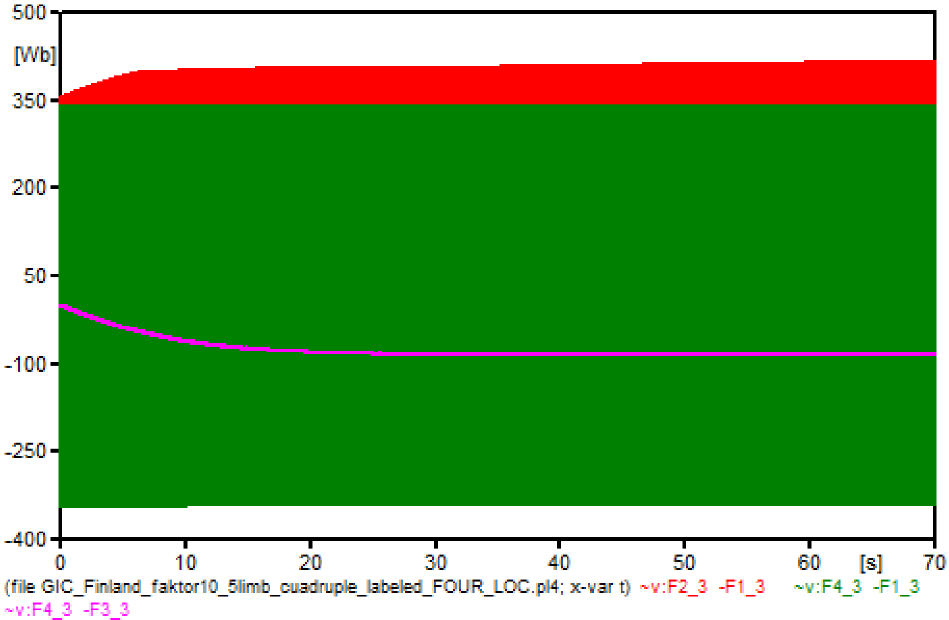

Figure E.1: Flux-linkages in different core sections, including the air path, of transformer T2 during the test at 200 A DC-current and LOC is 500 mH when using a 300MVA-3 w/Δ. The curves represents leg (red), yoke (green) and air path (pink).

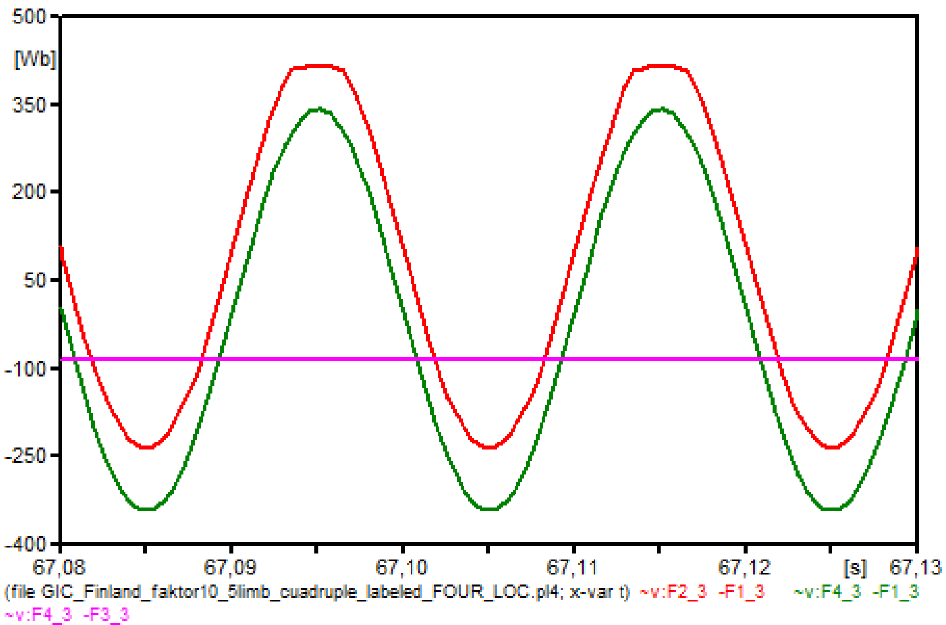

Figure E.2: Section of Figure E.1

.

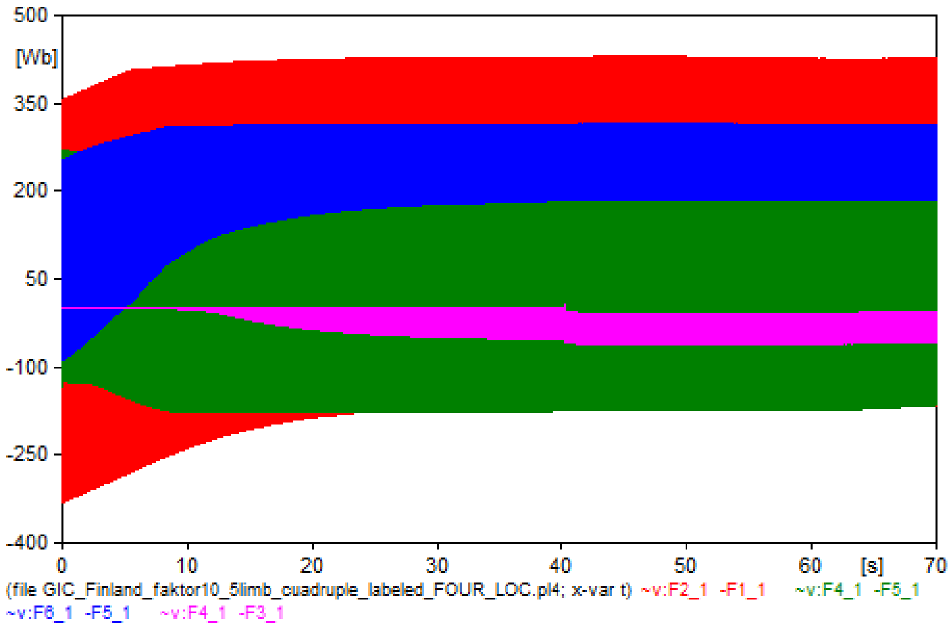

Figure E.3: Flux-linkages in different core sections, including the air path, of transformer T2 during the test at 200 A DC-current and LOC is 500 mH when using a 300MVA-5 w/Δ. The curves represents leg (red), yoke (green), outer limb (blue) and air path (pink).

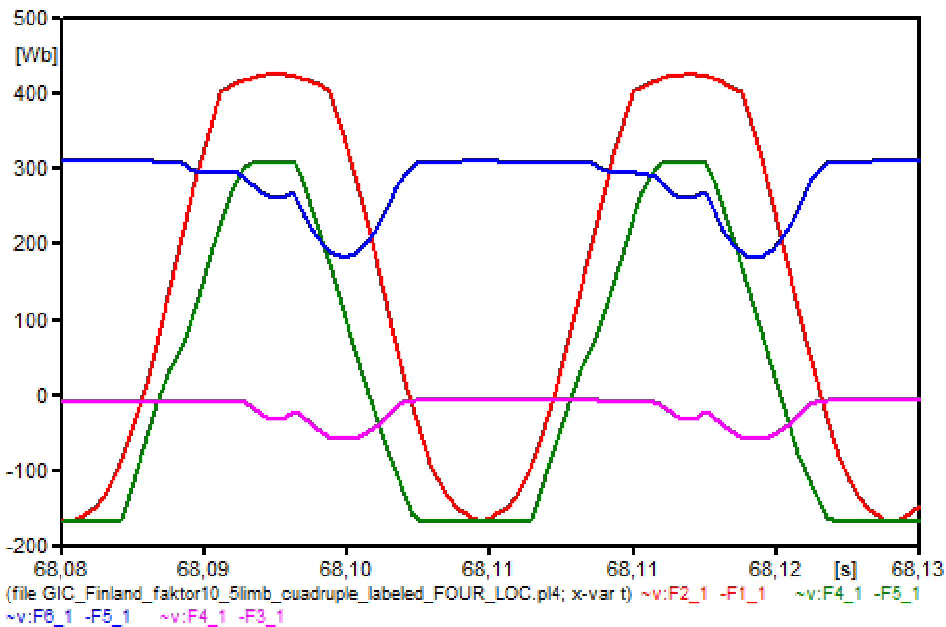

Figure E.4: Section of Figure E.3

.

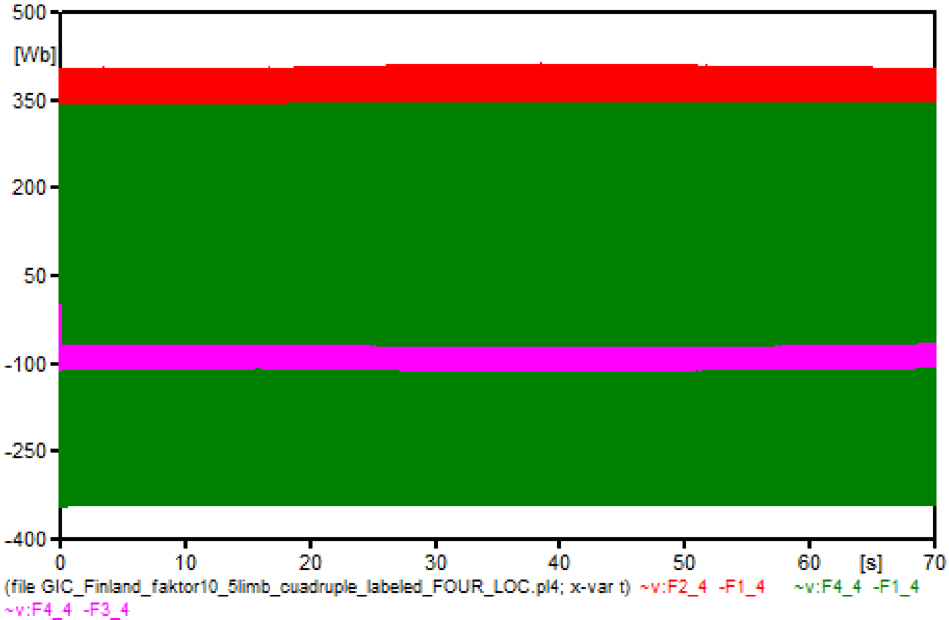

Figure E.5: Flux-linkages in different core sections, including the air path, of transformer T2 during the test at 200 A DC-current and LOC is 500 mH when using a 300MVA-3 w/o Δ. The curves represents leg (red), yoke (green) and air path (pink).

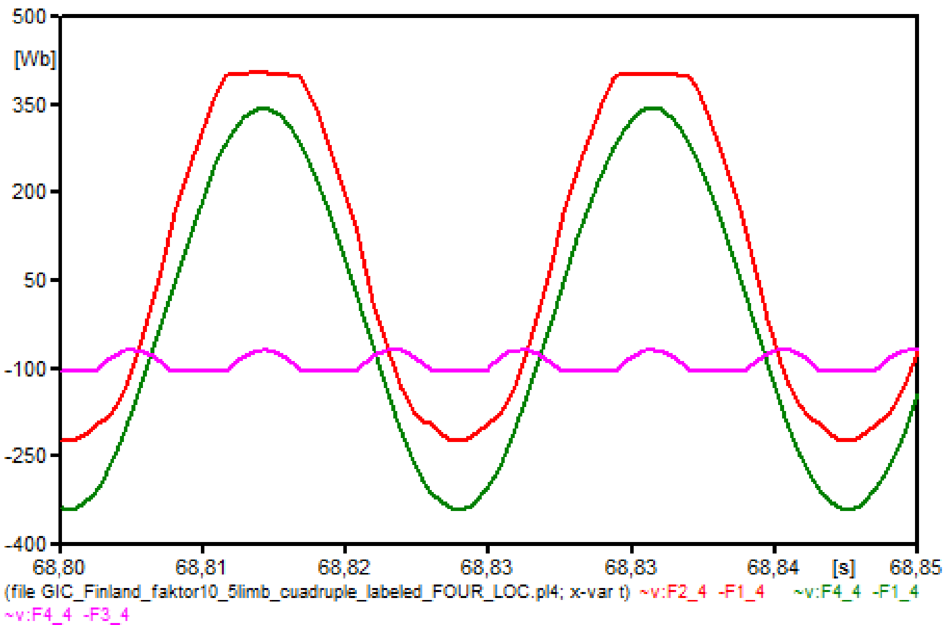

Figure E.6: Section of Figure E.5

.

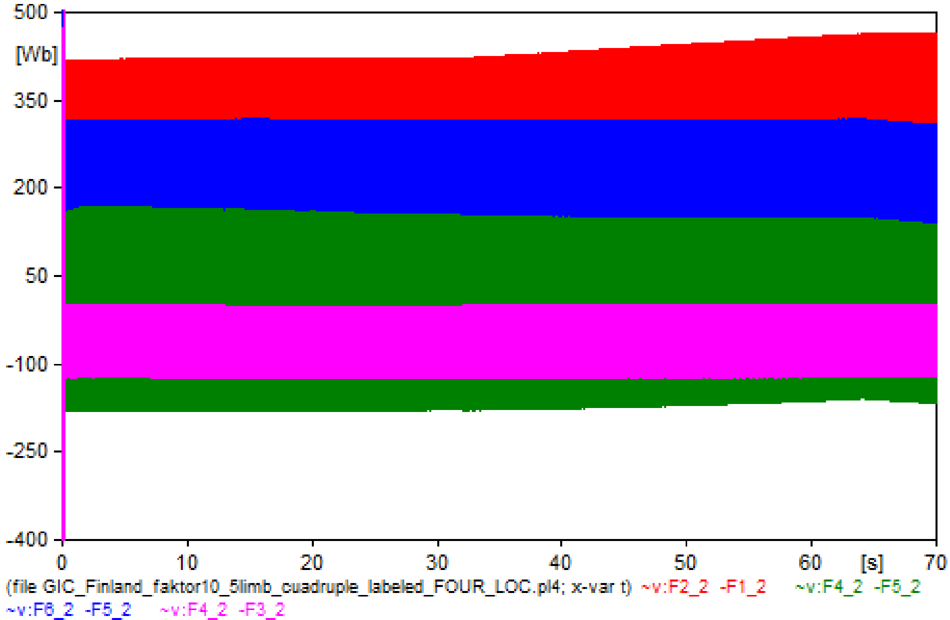

Figure E.7: Flux-linkages in different core sections, including the air path, of transformer T2 during the test at 200 A DC-current and LOC is 500 mH when using a 300MVA-5 w/o Δ. The curves represents leg (red), yoke (green), outer limb (blue) and air path (pink).

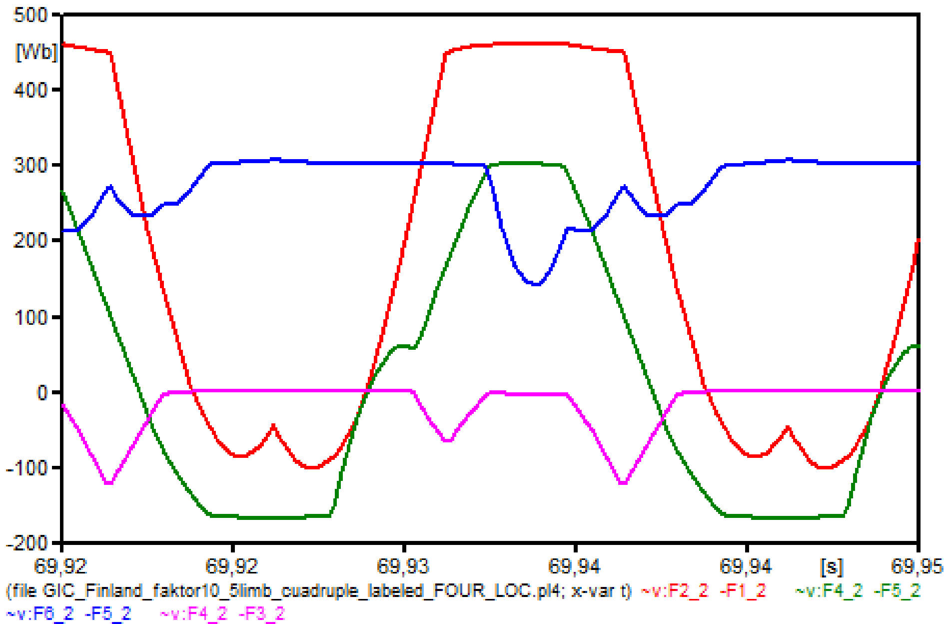

Figure E.8: Section of Figure E.7

.

Bibliography

Siemens AG. Geomagnetic induced currents, Accessed 11 Apr 2016 . URL http://www.energy.siemens.com/us/pool/hq/services/power-transmission-distribution/power-technologies-international/software-solutions/pss-e/GIC%20Module_FF%20120809.pdf.

A. Amberg and A. Rangel. Tutorial on symmetrical components part 2: Answer key. Report, Schweitzer Engineering Laboratories, Inc,, 2014.

National Earth Science Teachers Association. History of sunspot observations, Accessed 5 Apr 2016 . URL http://www.windows2universe.org/sun/activity/sunspot_history.html.

D. Baker, R. Balstad, J. M. Bodeau, E. Cemron, J. F. Fennell, and G. M. Fisher. Severe space weather events-understanding societal and economic impacts. Report, 2008.

C. Beck. The international e-pro report. Report, EPRO, 2013. URL http://www.ourenergypolicy.org/wp-content/uploads/2014/01/The-International-EPRO-Report.pdf.

C. Bergsåker. Impact of transformer core size on the reactive power requirement of power transformers due to gic. Report, 2014. URL http://www.diva-portal.se/smash/get/diva2:769799/FULLTEXT01.pdf.

E. E. Bernabeu. Modeling geomagnetically induced currents in dominion virginia power using extreme 100-year geoelectric field scenarios; part 1. *IEEE Transactions* *on Power Delivery*, 28(1):516–523, 2013. ISSN 0885-8977. doi: 10.1109/TPWRD.2012.2224141.

E. E. Bernabeu. Single-phase transformer harmonics produced during geomagnetic disturbances: Theory, modeling, and monitoring. *IEEE Transactions on Power Delivery*, 30(3):1323–1330, 2015. ISSN 0885-8977. doi: 10.1109/TPWRD.2014.2371927.

Wikipedia BillC, Accessed 5 Apr 2015 . URL https://upload.wikimedia.org/wikipedia/commons/thumb/6/64/Transformer3d_col3.svg/325px-Transformer3d_col3.svg.png.

N. Chiesa, A. Lotfi, H. K. Høidalen, B. A. Mork, Ø. Rui, and T. M. Ohnstad. Five-leg transformer model for gic studies.

National Research Council. *Severe Space Weather Events–Understanding Societal and Economic Impacts: A Workshop Report.* The National Academies Press, Washington, DC, 2008. ISBN 978-0-309-12769-1. doi: doi:10.17226/12507. URL http://www.nap.edu/catalog/12507/severe-space-weather-events-understanding-societal-and-economic-impacts-a.

E. F. Fuchs and M. A. S. Masoum. *Chapter 2 - Harmonic Models of Transformers A2 - Fuchs, Ewald F*, pages 55–108. Academic Press, Burlington, 2008. ISBN 978-0-12-369536-9. doi: http://dx.doi.org/10.1016/B978-012369536-9.50003-6. URL http://www.sciencedirect.com/science/article/pii/B9780123695369500036.

C. T. Gaunt. Reducing uncertainty – responses for electricity utilities to severe solar storms. *J. Space Weather Space Clim.*, 4:A01, 2014. URL http://dx.doi.org/10.1051/swsc/2013058.

J. L. Gilbert. Simplified techniques for treating the ocean-land interface for geomagnetically induced electric fields. In *Electromagnetic Compatibility (EMC), 2014 IEEE International Symposium on*, pages 566–569. doi: 10.1109/ISEMC.2014.6899035.

R. Girgis and K. Vedante. Effects of gic on power transformers and power systems. In *Transmission and Distribution Conference and Exposition (T&D),*

2012 IEEE PES, pages 1–8. ISBN 2160-8555. doi: 10.1109/TDC.2012.6281595. URL http://ieeexplore.ieee.org/ielx5/6267012/6281396/06281595.pdf?tp=&arnumber=6281595&isnumber=6281396.

Steele Hill/NASA, Accessed 5 Apr 2016 . URL http://www.cosmosportal.org/files/35201_35300/35204/file_35204.gif.

H. K. Høidalen. Atpdraw, Accessed 12 apr 2016 . URL http://www.atpdraw.net/.

H. K. Høidalen, B. A. Mork, F. Gonzalez, D. Ishchenko, and N. Chiesa. Implementation and verification of the hybrid transformer model in atpdraw. *Electric Power Systems Research*, 79(3):454–459, 2009. ISSN 0378-7796.

IEEE. Ieee guide for establishing power transformer capability while under geomagnetic disturbances. *IEEE Std C57.163-2015*, pages 1–50, 2015. doi: 10.1109/IEEESTD.2015.7286929.

M. Lahtinen and J. Elovaara. Gic occurrences and gic test for 400 kv system transformer. *IEEE Transactions on Power Delivery*, 17(2):555–561, 2002. ISSN 0885-8977. doi: 10.1109/61.997938. URL http://ieeexplore.ieee.org/ielx5/61/21528/00997938.pdf?tp=&arnumber=997938&isnumber=21528.

Store norske leksikon. Sola, Accessed 5 Apr 2016 . URL https://snl.no/Sola.

C. M. Liu, L. G. Liu, and R. Pirjola. Geomagnetically induced currents in the high-voltage power grid in china. *IEEE Transactions on Power Delivery*, 24(4):2368–2374, 2009. ISSN 0885-8977. doi: 10.1109/TPWRD.2009.2028490.

J. A. Marusek. Solar storm threat analysis. Report, 2007. URL http://www.breadandbutterscience.com/SSTA.pdf.

M. Myllys, A. Viljanen, Ø. A. Rui, and T. M. Ohnstad. Geomagnetically induced currents in norway: the northernmost high-voltage power grid in the world. *J. Space Weather Space Clim.*, 4:A10, 2014. URL http://dx.doi.org/10.1051/swsc/2014007.

NASA. Cme week: The difference between flares and cmes, Accessed 5 Apr 2016 a. URL https://www.nasa.gov/content/goddard/the-difference-between-flares-and-cmes.

NASA. The sun's layers and temperatures, Accessed 5 Apr 2016 b. URL http://nmp.jpl.nasa.gov/st5/SCIENCE/sun.html.

NASA. The sunspot cycle, Accessed 5 Apr 2016 c. URL http://solarscience.msfc.nasa.gov/SunspotCycle.shtml.

NASA. What is a solar flare?, Accessed 5 Apr 2016 d. URL http://hesperia.gsfc.nasa.gov/sftheory/flare.htm.

NASA. Geomagnetic disturbances: Their impact on the power grid. *IEEE Power and Energy Magazine*, 11(4):71–78, 2013. ISSN 1540-7977. doi: 10.1109/MPE.2013.2256651.

D. Negri and M. Gotti. Transformer model benchmarking. Report, Politecnico di Milano and NTNU, 2007.

NERC. Application guide - computing geomagnetically-induced current in the bulk-power system. Report, 2013.

NOAA/SWPC. Planetary k-index, Accessed 5 Apr 2016 . URL http://www.swpc.noaa.gov/products/planetary-k-index.

P. R. Price. Geomagnetically induced current effects on transformers. *Power Delivery, IEEE Transactions on*, 17(4):1002–1008, 2002. ISSN 0885-8977. doi: 10.1109/TPWRD.2002.803710. URL http://ieeexplore.ieee.org/ielx5/61/22435/01046876.pdf?tp=&arnumber=1046876&isnumber=22435.

R. Thorberg. Risk analysis of geomagnetically induced currents in power systems. Report, 2012. URL http://www.iea.lth.se/publications/MS-Theses/Full%20document/5296_full_document_GIC.pdf.

K. Zheng, L. Trichtchenko, R. Pirjola, and L. G. Liu. Effects of geophysical parameters on gic illustrated by benchmark network modeling. *IEEE Transactions on Power Delivery*, 28(2):1183–1191, 2013. ISSN 0885-8977. doi: 10.1109/TPWRD.2013.2249119.

A. Ádám, E. Prácser, and V. Wesztergom. Estimation of the electric resistivity distribution (eurhom) in the european lithosphere in the frame of the eurisgic wp2 project. *Acta Geodaetica et Geophysica Hungarica*, 47(4):377–387, 2013. ISSN 1587-1037. doi: 10.1556/AGeod.47.2012.4.1. URL http://dx.doi.org/10.1556/AGeod.47.2012.4.1.